TEAMER
Testing & Expertise for Marine Energy

Post Access Report

Development of an advanced wave-to-wire OWC model in WEC-Sim

Awardee: Mondragon University

Awardee point of contact: Markel Peñalba

Facility: WEC-Sim

Facility point of contact: Jorge Leon-Quiroga

Date: 11/22/2024

EXECUTIVE SUMMARY

Accurate numerical models are crucial for the development of wave energy converter (WEC) technologies, providing the means for power production and lifetime assessment, site selection, and design of mooring lines, PTO systems and controllers, among other aspects. The present project aims at developing a wave-to-wire numerical model for floating oscillating water column (OWC) devices based upon the Wave Energy Converter SIMulator (WEC-Sim) platform. To that end, nonlinear hydrodynamics, considering viscous and nonlinear Froude-Krylov effects were implemented, and new capabilities were articulated into the WEC-Sim platform, incorporating thermos-aerodynamic effects for the air-turbine. A numerical model of a wave-to-wire controller was developed in this project, and its efficiency and performance have been tested numerically. In addition to this, a mooring system was also included in the numerical model. The hydrodynamic coefficients for the OWC were calculated using different numerical solvers: ANSYS, WAMIT, Capyatine, and NEMOH. This report also contrasts two distinct modeling approaches. In the first approach, the WEC's main structure and the OWC are modeled as separate entities. In the second, the WEC and OWC are considered a single body, with the free surface of the oscillating water column added as an extra degree of freedom. Nonlinear hydrodynamic effects, including viscosity and nonlinear Froude-Krylov forces, are incorporated to assess their impact on the numerical analysis of OWC systems.

1 INTRODUCTION TO THE PROJECT

Mondragon University (Mondragon Goi Eskola Politeknikoa - MGEP) has developed a numerical model for an oscillating water column (OWC) wave energy converter (WEC), designed by IDOM, a multi-national corporation which provides consulting, engineering, and architecture services in Spain and internationally, that includes the hydrodynamics and the power take-off (PTO) dynamics. Previous work has shown some discrepancies between Mondragon's numerical modeling approach and that observed in Wave Energy Converter SIMulator (WEC-Sim). The discrepancies include the motion of the floater in different degrees of freedom, particularly roll and pitch, and the motion of the water column. These discrepancies, especially the one related to the water column, results in significant differences in the power production assessment and mooring loadings, both of which are crucial aspects for the design of the WEC. The currently available numerical models, developed by Mondragon, do not have the capacity to capture all the relevant hydrodynamics and PTO dynamics. These models are limited by their original implementation and cannot be extended to include more complex dynamics related to nonlinear hydrodynamics, and PTO dynamics and losses.

A prior Mondragon collaborator, Giorgi et al. [1] developed a numerical model to predict the performance of spar-buoy OWCs (*i.e.*, floating OWCs)—an example of which is shown in Figure 1—and validated the predictions using experimental results. The experimental setup used a slack-mooring system attached to the wave tank floor, and the turbine model in both the experimental and numerical work was replaced with an orifice model. The geometry used in [1] and in the current study follows one of the optimal designs reported in [2].

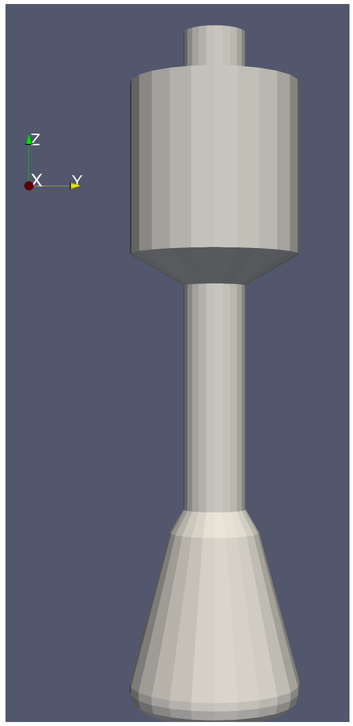

Figure 1: The spar-buoy (floating) OWC WEC used in this study

The main objective of this project is to create a reliable and efficient numerical platform based on WEC-Sim, to include nonlinear hydrodynamics, the most relevant PTO features and dynamics, nonlinear mooring dynamics, and integration of control algorithms in the model. The final WEC-Sim model was used to study the performance of the air turbine, and it was also used to study energy maximizing control algorithms. The outcomes of this project are performance results from a WEC-Sim model that includes nonlinear hydrodynamics, mooring line dynamics, and PTO dynamics and inefficiencies of an OWC. The key performance indicators (KPI) related to this project are the motion of the system (relative heave between the floater and the water column, and roll and pitch motions), power production (pneumatic and electric power) and mooring line tension. The results from this work will have a direct impact on MGEP's future research and development efforts because the model will allow them to simulate the wave-to-wire dynamics of the proposed system. This WEC-Sim model can be used as a readily available numerical platform to model and evaluate complex control algorithms for floating OWC devices, which are crucial to improve power generation.

2 ROLES AND RESPONSIBILITIES OF PROJECT PARTICIPANTS

Mondragon University actively participated in the development of the WEC-Sim wave-to-wire model. On the one hand, MGEP provided the necessary data for the definition of the case study with the information of the floating OWC device, including geometry, hydrodynamic coefficients, mooring lines and PTO system

The experimental results include time series of free surface elevation and device motion under different conditions. On the other hand, MGEP assisted with the implementation of the model by collaborating with NREL and Sandia on the development of the mooring and PTO models and the selection of the numerical solvers. Finally, MGEP suggested a set of relevant test cases, considering lifetime and power production assessment, to evaluate the gain in accuracy against computational demand when using the novel WEC-Sim wave-to-wire model.

2.1 APPLICANT AND FACILITY RESPONSIBILITIES AND TASKS PERFORMED

The task and responsibilities for this project are listed below:

- **Task 1: Review of existing numerical model of IDOM's OWC**
  - Mondragon University:
    - Provided their existing numerical model with all relevant documentation that facilitated the review, including prior Ansys Aqwa and WAMIT runs.
  - WEC-Sim:
    - Reviewed the existing documentation
    - Reviewed model properties
    - Determined additional inputs and files needed to implement the advanced features in WEC-Sim
    - Built a WEC-Sim model that includes the base features, i.e. a linear hydrodynamic model, that currently exist in the current Mondragon numerical model.
    - Defeatured the device geometry
    - Created a mesh of the device geometry
    - Run the BEM software simulations in WAMIT, NEMOH and Capytaine
    - Compared the BEM results from different approaches to model the OWC
    - Compared outputs from the base WEC-Sim model against the existing Mondragon model to understand where the two models diverge.
- **Task 2: Implementation of nonlinear hydrodynamics**
  - Mondragon University:
    - Provided the dimensions of the device.
  - WEC-Sim:
    - Generated a mesh of the device geometry that was exported in the .stl mesh format required by WEC-Sim
    - Completed a mesh sensitivity study to determine the appropriate mesh size to generate accurate hydrodynamic forces while not comprising computational speed.

    * Compared the linear WEC-Sim model to the nonlinear WEC-Sim model to identify where the solutions begin to diverge.

- **Task 3: Implementation of nonlinear mooring dynamics**
  - Mondragon University:
    * Defined the relevant properties necessary to implement nonlinear mooring simulations using MoorDyn.
  - WEC-Sim:
    * Defined inputs required to run MoorDyn
    * Determined number of nodes to define catenary mooring for desired model accuracy
    * Completed a wave height sensitivity study to ensure convergence of dynamics with MoorDyn.
- **Task 4: Implementation of advanced PTO dynamics**
  - Mondragon University:
    * Provided the PTO parameters, in addition to the existing PTO model.
  - WEC-Sim:
    * Defined PTO parameters and level of fidelity.
    * Updated the model to include advanced PTO dynamics.
    * Verified simulation outputs based on PTO inputs.
- **Task 5: Implementation of a feedback control system**
  - Mondragon University:
    * Provided feedback to the WEC-Sim team for implementation of the feedback control in the simulation.
  - WEC-Sim:
    * Defined the control parameters that were implemented within the WEC-Sim framework. A preliminary version included the PTO and control via a simplified model based on an orifice equation. The control parameter in this case was just a damping parameter.
    * Built an WEC-Sim numerical model that allows Mondragon University to implement and test different control algorithms on the advanced PTO model
- **Task 6: Final report and Tech Transfer**
  - Mondragon University:
    * Collaborated with WEC-Sim on development of the Post Access Report and participate in a Tech Transfer meeting
    * Submitted Post Access Report and data to MHKDR
  - WEC-Sim:

* Hosted technology transfer meeting with Mondragon University. During this meeting, the WEC-Sim team went through the work completed during the TEAMER award, and answered questions from the Mondragon Team.
* Provided the following to DOE Office of Scientific and Technical Information (OSTI)
* An initial abstract suitable for public release at the time of the CRADA is executed.
* A final report, within thirty (30) days upon completion or termination of this CRADA, to include a list of Subject Inventions.
* Other scientific and technical information in any format or medium that is produced as a restore of this CRADA

3 PROJECT OBJECTIVES

The main objective of this project is to create a reliable and efficient numerical platform to simulate an OWC. The model was developed in WEC-Sim, including nonlinear hydrodynamics, relevant PTO features and dynamics, nonlinear mooring dynamics, and integration of control algorithms in the model. This numerical model was developed to study the performance of the air turbine, and the energy maximizing control algorithms. The proposed task and the specific approach to achieve the objectives are described below:

1. **Develop a Comprehensive Numerical Platform for OWC Simulation:**
   Create a reliable and efficient numerical model in WEC-Sim incorporating nonlinear hydrodynamics, relevant PTO features and dynamics, nonlinear mooring dynamics, and control algorithm integration.
2. **Enhance Numerical Models through Existing Design Review:**
   Review and refine the OWC design, including mass properties, hydrodynamic coefficients, PTO details, and mooring configurations, to develop an initial linear hydrodynamic model.
3. **Incorporate Nonlinear Hydrodynamic Effects:**
   Integrate advanced hydrodynamic features such as nonlinear hydrostatics and Froude-Krylov forces.
4. **Integrate Nonlinear Mooring Dynamics:**
   Implement nonlinear mooring models using tools like MoorDyn..
5. **Advance PTO Dynamics Modeling:**
   Incorporate air turbine PTO dynamics into the WEC-Sim model, either through WEC-Sim's PTO-Sim library or custom Simscape-based development, ensuring accurate power generation and system response.
6. **Develop and Implement Feedback Control Systems:**
   Build control systems to evaluate advanced strategies, enabling user customization and testing of various algorithms to maximize energy extraction.

7. **Facilitate Knowledge Transfer and Documentation:**
   Provide detailed reports, host technology transfer meetings, and deliver technical outputs to collaborators and the TEAMER to ensure effective dissemination and application of the developed tools and methodologies.

4 TEST FACILITY, EQUIPMENT, SOFTWARE, AND TECHNICAL EXPERTISE

NREL and Sandia jointly develop, validate, and disseminate the WEC-Sim open-source software. The software is developed in MATLAB/Simulink using the multi-body dynamics solver Simscape Multibody. WEC-Sim has the ability to model devices composed of bodies, joints, power take-off systems, and mooring systems. Simulations are performed in the time-domain by solving the governing wave energy converter equations of motion in the six Cartesian degrees of freedom. The model can be used to simulate WEC device dynamics and performance in operational and extreme waves, allowing for improvement of WEC performance during the design process.

5 TEST OR ANALYSIS ARTICLE DESCRIPTION

The Mondragon OWC, referred to as the MARMOK technology, is a spar-like floating OWC device that harnesses the energy from ocean waves by converting the motion of the water column within the buoy into pneumatic energy first, and electricity afterwards. Both motions of the water column cause the rotation of the air turbine installed on the top of the buoy, as illustrated in Figure 2, which rotates the turbine in the same direction regardless of the direction of the air flow.

The buoy is moored to the seabed by means of four catenary-like mooring lines, as shown in Figure 3 and Table 1, ensuring the station keeping of the device. IDOM has developed this device during the last 10 years, which has been tested in the open ocean, i.e. off the Basque coast in Spain, for over a year, including two harsh winters with extreme waves of up to 14m. Therefore, the device has demonstrated its reliability and IDOM is now further developing the device in order to reduce its levelized cost of energy (LCoE).

The energy conversion is carried out through a bidirectional turbine, as the one shown in Figure 4, which is, in turn, coupled to an electric generator. This turbine is a well-known Wells turbine, specifically designed for OWC wave energy devices. In the case of the MARMOK device, an advanced PTO system is currently being developed, including the turbine with additional control actuators and an electric generator designed ad-hoc.

The numerical tests conducted during this project enabled significant advances on the design of the floating structure, mooring lines and the PTO system for wave energy converters in general, and OWC devices specifically.

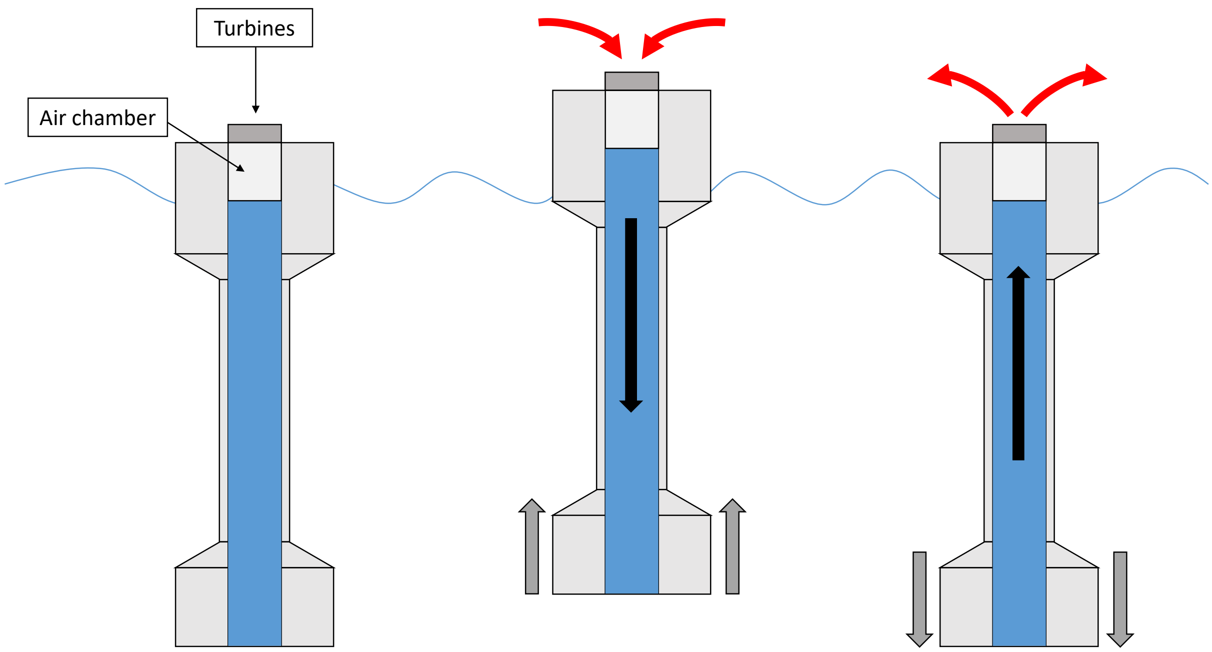

Figure 2: Working principles of a floating OWC wave energy converter.

Mooring system parameters at full scale, considering the different locations of the fairlead for configurations D1 and D2.

Parameter	Value
Line diameter, d_L [mm]	32
Net line linear density, w_L [kg m^{-1}]	34.82
Jumper mass, m_J [kg]	4030.46
Jumper density, ρ_J [kg m^{-3}]	123.00
Clump-weight mass, m_C [kg]	36139.83
Clump-weight density, ρ_C [kg m^{-3}]	8097.50
Length of line anchor-jumper, L_1 [m]	143.28
Length of line jumper-clump-weight, L_2 [m]	37.01
Length of line fairlead-clump-weight, L_3 [m]	50.40
Anchor radius, r_A [m]	211.2
Anchor z-coordinate, z_A [m]	−80
Fairlead radial coordinate, r_F [m]	9.28
Fairlead z-coordinate (config. D1), $z_{F,1}$ [m]	−0.82
Fairlead z-coordinate (config. D2), $z_{F,2}$ [m]	−2.58

Table 1: Mooring parameters Giorgi et al. [1]

6 WORK PLAN

WEC-Sim is a mid-fidelity WEC numerical modelling tool based on linear potential flow theory. Hence, the wave field is considered to be a linear superposition of incident, radiated and diffracted regular wave components. Boundary Element Method (BEM) software are used to compute a body's hydrodynamic coefficients (e.g. added mass, damping, excitation force) for a range of discrete frequencies. WEC-Sim's Boundary Element Method Input/Output (BEMIO) is then used to pre-process the hydrodynamic coefficients

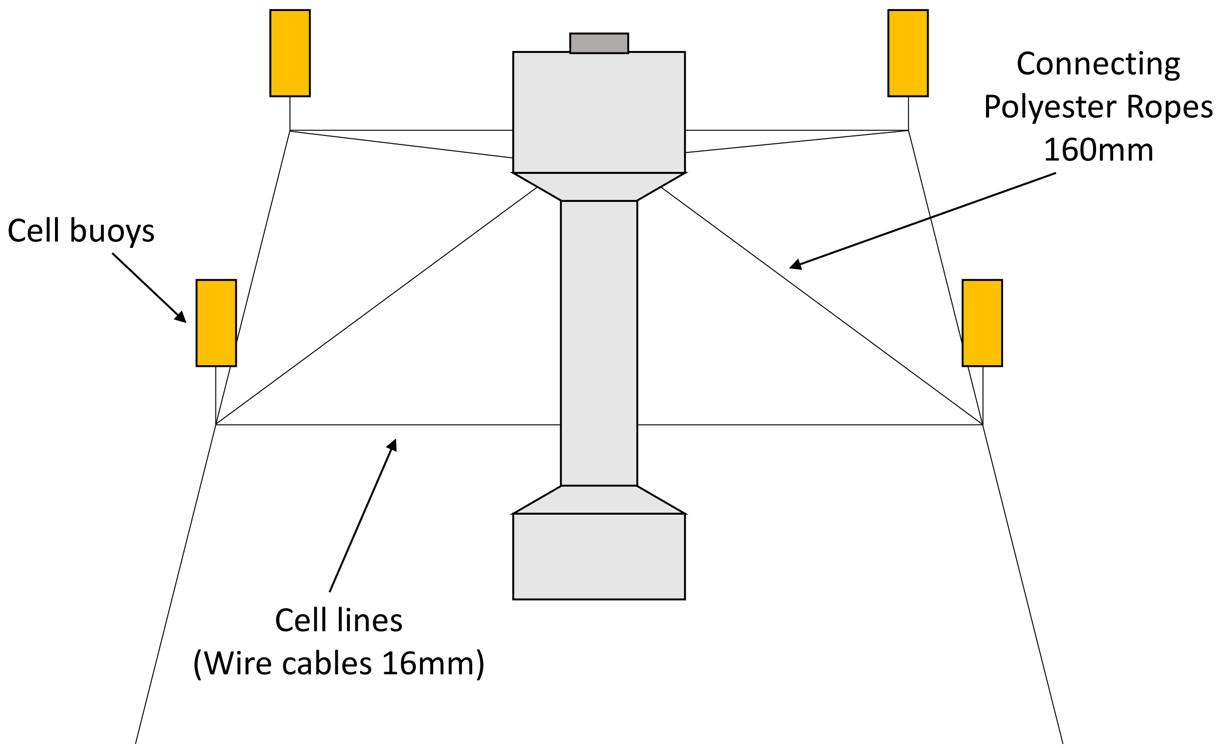

Figure 3: Mooring line configuration of IDOM's MARMOK device, with an iso-view where the cell buoys are floating at the surface.

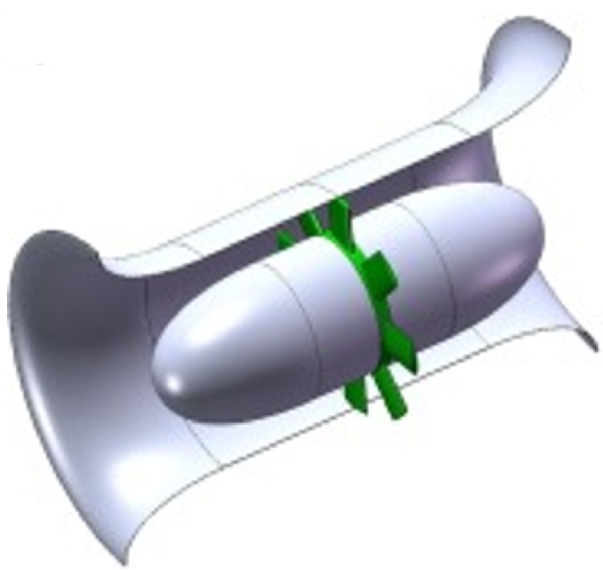

Figure 4: Bi-directional Wells turbine for OWC devices.

and save them to a **.h5* file, the format that is read by WEC-Sim. WEC-Sim then converts these frequency domain coefficients into their time-domain formulations (i.e. impulse response functions) to calculate the hydrodynamic forces. This conversion is required to model the WEC system in the time-domain, which is necessary to include non-linearities in the system - such as joints, PTOs, control systems, moorings etc. A complete description of the software's theory is available on the WEC-Sim website: `https://wec-sim.github.io/WEC-Sim/main/theory/index.html` The accuracy of WEC-Sim has been verified in code-to-code comparisons and validated against experimental data. A full list of relevant publications is also available online: `https://openei.org/wiki/PRIMRE/Signature_Projects/WEC-Sim`.

6.1 NUMERICAL MODEL DESCRIPTION

The numerical model for this project was developed in WEC-Sim, an open-source simulation tool designed for modeling wave energy converters (WECs). The model integrates several advanced features, including nonlinear hydrodynamics, nonlinear mooring dynamics, and a detailed power take-off (PTO) system. Hydrodynamic forces are calculated using the BEM results integrated within WEC-Sim. The model was enhanced by the implementation of nonlinear hydrostatics and Froude-Krylov forces. The PTO system model allows dynamic torque and power calculations and the possibility of modeling control algorithms. Nonlinear mooring dynamics are incorporated using MoorDyn, a tool for simulating mooring line dynamics.

6.2 SAFETY

The project did not require any in-person or physical testing. The numerical analysis was completed as a desktop study. Applicable office safety standards were be followed.

6.3 CONTINGENCY PLANS

This project did not have any major risks to project completion. The project did not experience any major delays in execution or greater effort (and budget) on specific tasks. It is important to mention the extended time for DOE approval, which was expected from the beginning because Mondragon University is an institution based outside the United States.

6.4 DATA MANAGEMENT

WEC-Sim-generated data was stored locally on the machines the software was run on and backed up using OneDrive (up to 1TB available). The final dataset containing results from the numerical modelling campaign will be uploaded to MHKDR while a GitHub repository was used for version tracking.

6.5 DATA PROCESSING

WEC-Sim saves the data from each run as a **.mat* file (binary), which can be read into memory with MATLAB or Python for post-processing. Meaningful directory and file names have been used for clarity and figures have been provided with accompanying post processing scripts attached for complete traceability and reproducibility.

6.6 DATA ANALYSIS

All the outputs from the numerical model were post processed in MATLAB. The data has been saved in the **.mat* format, which is the standard for MATLAB. The metrics that were studied in the model include the pressure in the air chamber, and the power in the different subsystems of the PTO power conversion chain such as the air turbine and electric generator. Some other variables that the model can calculate are the relative position of the OWC, its velocity, and acceleration.

7 PROJECT OUTCOMES

The main objective of this project was to create a reliable and efficient numerical platform based on WEC-Sim, to include nonlinear hydrodynamics, the most relevant PTO features and dynamics, nonlinear mooring dynamics, and integration of control algorithms in the model. The WEC-Sim team was provided an existing model of the IDOM OWC WEC developed by Mondragon University. First, the team investigated the model and discussed with Mondragon to derive a plan for improving the model. Next, the team applied nonlinear hydrodynamics, developed aerodynamics approximations, selected and modeled a turbine, and implemented advanced control techniques. Lastly, the results of the model improvement in terms of the performance and validation were presented and handed off back to Mondragon University.

7.1 INITIAL MODEL INVESTIGATION

The team investigated the initial WEC-Sim model provided by Mondragon to understand the state of work and identify areas of improvement. The model consisted of two hydrodynamic bodies, one of which represented the floater and the other represented the oscillating water column. The hydrodynamic coefficients for Mondragon provided model were calculated using both WAMIT and Ansys Aqwa by assuming both are rigid bodies and inputting the body meshes. The team proceeded with the results from Ansys Aqwa as they produced a more stable model, free from unexpected peaks at irregular frequencies. The power take-off dynamics were defined as a simple translational spring and damping force applied to the relative motion between the two bodies. The mooring was also defined as a simple spring and damping force in 6 degrees of freedom using WEC-Sim mooring matrix formulation. The two-body approach used to model the OWC can be effective as a simple representation of the dynamics, but is not truly accurate because the water column consists of compressible air rather than a rigid body. Nevertheless, the initial model was functional and sufficient for beginning the project.

In order to understand the limitations of the existing model, the model results were compared to a paper by Giorgi et al. [1] which modeled the same WEC and compared with the experimental data. Although the team did not have access to the experimental data directly, comparing to the plots in the paper allowed the team to match the general trends of the experimental data. First, when comparing the existing WEC-Sim model to the paper, it was clear that Mondragon has modeled the D2 configuration from the paper, with a center of gravity of -31.96 m. This configuration is shown in Figure 9. Mondragon's model was missing a few factors which are required to ensure consistency between comparisons. First, the mooring system needed to be defined using MoorDyn. The paper provided a very detailed description of the mooring system, which made the process of developing the MoorDyn model component relatively straightforward.

The team also implemented nonlinear dynamics, viscous drag forces, and power take-off forces according to the paper. WEC-Sim provides nonlinear hydrodynamics settings that can be configured using the parameter `body(ii).nonlinearHydro` in the input file. These settings enable the integration of wave pressure across the surface of the body, enhancing the accuracy of buoyancy and Froude-Krylov force calculations. There are two options for configuring nonlinear hydrodynamics:

- **Option 1:** Setting `body(ii).nonlinearHydro = 1` calculates the wave pressure by integrating based on the mean wave elevation and the instantaneous position of the body. This option provides a simplified approach that considers changes in body position relative to the mean wave surface.
- **Option 2:** Setting `body(ii).nonlinearHydro = 2` calculates the wave pressure by integrating based on the instantaneous wave elevation and the instantaneous position of the body. This method captures a higher level of nonlinearity and is recommended when more precise nonlinear effects need to be accounted for in the simulation.

Using these nonlinear hydrodynamics option allows WEC-Sim to account for variations in wave pressures more effectively, resulting in improved modeling of wave-structure interactions.

The nonlinear dynamics were turned on by setting $body(1).nonlinearHydro = 1$ in the WEC-Sim input file (only applied to floater). The viscous drag forces were selected according to the estimated drag coefficients and areas for the estimated projected shape in each direction. Lastly, the power take-off forces were applied as a custom forcing function according to the following equation.

After including the nonlinear dynamics, viscous drag forces and PTO force, the model results could be compared to the results from the paper. Initial comparisons found instability in the WEC-Sim model associated with the calculation of nonlinear forces. The mesh used was likely not small enough to produce reliable results. Thus, the team turned the nonlinear options off here for comparisons and this option was revisited later. The results from the paper are shown in Figure 5 for a wave period of 10.2 s and a height of 5.1 m (Giorgi et al. [1]). Based on estimates, the amplitude of displacement for the experimental results is about 2.5 m, 10 degrees, and 5 degrees in heave, roll, and pitch, respectively. Figure 6 shows the initial results of

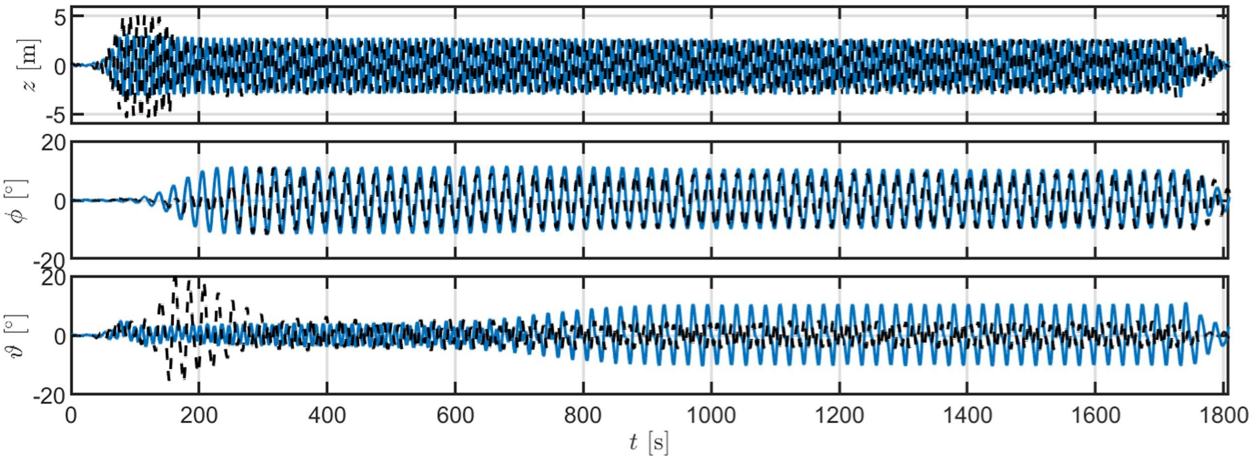

Figure 5: Validation plot from Giorgi et al. [1] for a wave period of 10.2 s and a height of 5.1 m. Model results shown by the blue solid line and the experimental results shown by the black dashed line.

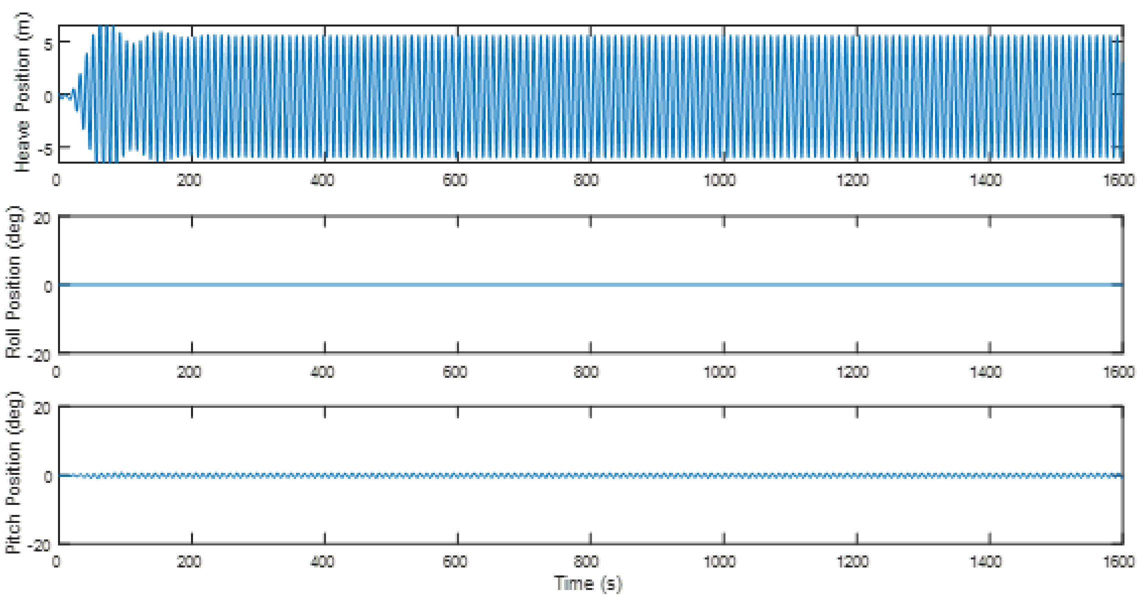

Figure 6: WEC-Sim run with nonlinear dynamic effects for for a wave period of 10.2 s and a height of 5.1 m

the WEC-Sim model in each of the respective degrees of freedom. It is very apparent that the WEC-Sim model does not really match the results from the paper. The WEC-Sim results have amplitudes of displacement of about 5 m, 0 degrees, and 1 degree in heave, roll, and pitch, respectively. These discrepancies in the results are relatively large, but it is important to acknowledge that this is just an initial model.

The team investigated the initial model, completed literature review, and discussed with Mondragon to identify the following primary areas of improvement:

- Nonlinear hydrodynamics
- Improve mesh resolution and stabilize nonlinear model.
- Enhanced water column aerodynamics
- In order to develop a more accurate model, generalized body modes can be explored for representing the water column.
- Specific OWC turbine selection
- The specific turbine used has an impact on the simulation results and should be included in the model.
- Advanced control techniques
- Multiple control techniques should be explored to maximize electrical power.

7.2 NONLINEAR HYDRODYNAMICS

Nonlinear hydrodynamics were implemented using WEC-Sim's built-in feature that calculates the buoyancy and Froude-Krylov forces based on the instantaneous wave elevation and body position. The pressure on each panel of the **.stl* mesh is integrated to calculate the nonlinear forces at each time-step. This method requires a relatively fine mesh to accurately assess the nonlinear forces. For instance, the mesh provided by Mondragon did not seem to be good enough quality and lead to the instabilities when nonlinear hydrodynamics were applied. Figure 8 shows the heave response and 7 shows the surge response of the WEC, which illustrates a constant drifting behavior and the heave response is also impacted accordingly. For a symmetric body, the surge forces should not lead to an asymmetrical drift, so this response was deemed non-physical and is an issue with the model.

On the other hand, a finer mesh can lead to better results but also leads to a higher computation time. Using CUBIT, the team investigated multiple finer mesh discretizations in order to determine a result which is more appropriate for this geometry. Unfortunately, even with a very fine mesh, the team found a constant drifting force in both surge and yaw directions. The WEC-Sim team explored multiple options to mitigate the drift including damping and stiffness terms in surge and yaw degrees of freedom to maintain the equilibrium position at 0. The damping and stiffness terms limited the motion in these degrees of freedom but also led to further instabilities in the model. Regardless of the mesh resolution employed, the nonlinear hydrodynamics seemed to have significant issues which led to non-physical responses and instabilities in the model. Thus, the team decided to stick with the linear model for the initial analysis and consider nonlinearities later if necessary.

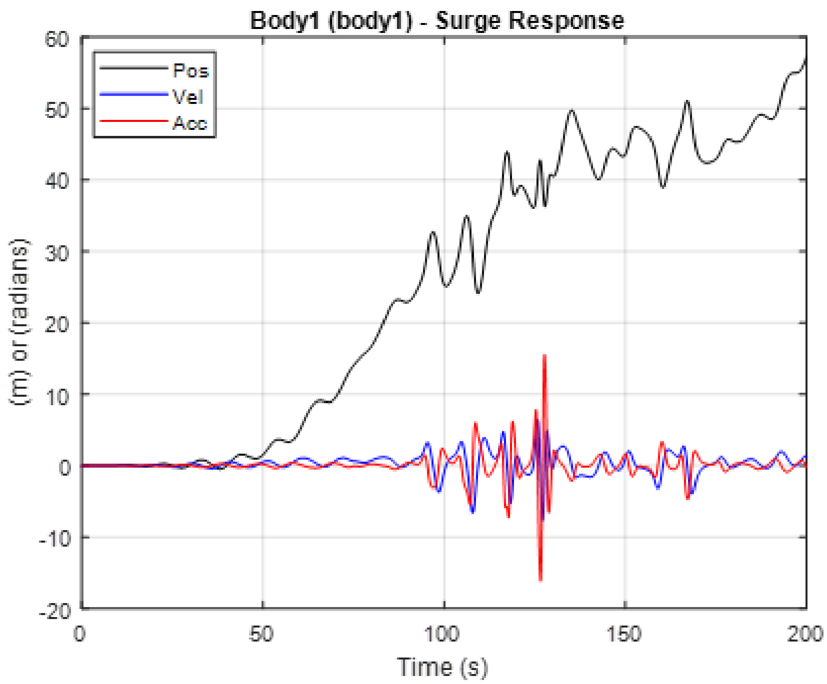

Figure 7: WEC-Sim surge behavior (nonlinear)

7.3 ENHANCED WATER COLUMN AERODYNAMICS - GENERALIZED BODY MODE APPROACH

Mondragon's OWC original model used a two-body approach. Although this method can be effective, it treats the oscillating water column as a rigid body instead of an air column. Instead, the WEC-Sim team created a new model which uses WAMIT to treat the water column as a generalized body mode (GBM).

In the GBM approach, additional degrees of freedom can be added to the WAMIT simulation to represent specific physical conditions of the system that will be modeled. The additional degrees of freedom are defined by the user to described a variety of modes of motion that can be represented by a specific normal velocity distribution on the body surface. Examples include structural deformations, motions of hinged bodies and oscillating water columns, among others. The steps to develop the WEC-Sim simulation are explained in detail in the following subsections: 1. Geometry Creation; 2. Mesh Development; 3. WAMIT Simulation; 4. WEC-Sim implementation; 5. Non-linear hydrodynamics.

7.3.1 Geometry Creation

The geometry used for the GBM approach was created based on the information available in the study by Davidson et al., 2021 [3], which is the same device from the work by Giorgi et al. [1]. The work by

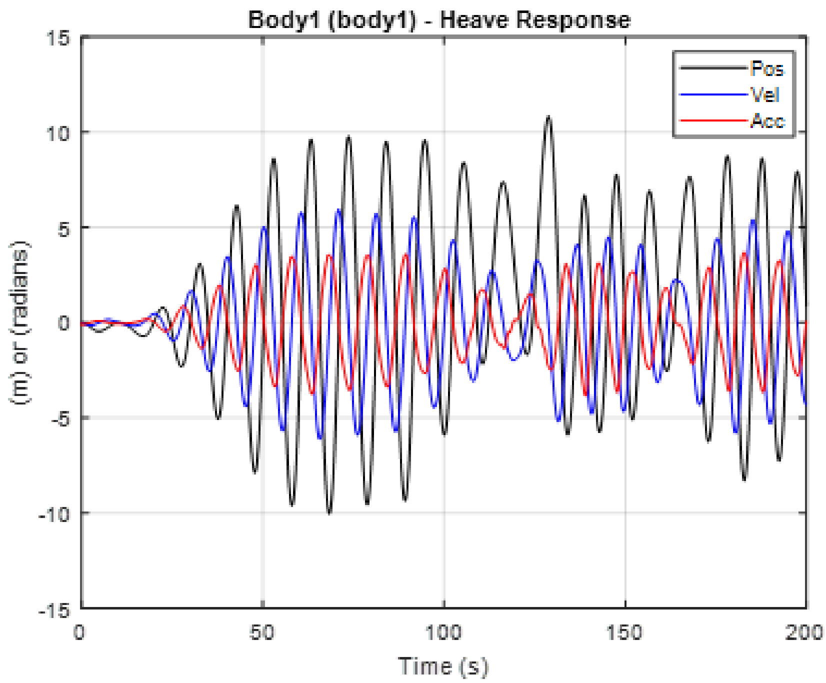

Figure 8: WEC-Sim heave behavior (nonlinear)

Physical characteristics of the Spar-buoy OWC model, for the two mass distributions considered.

Parameter	Config. D1	Config. D2
Buoy diameter, d_1 [m]	16.00	16.00
OWC diameter, d_2 [m]	5.89	5.89
Total length [m]	64.06	64.06
Floater section draft l_1 [m]	6.17	7.91
Buoy draft, l_s [m]	49.17	50.91
Air chamber height, l_c [m]	14.89	13.15
z-coordinate of CoB, z_B [m]	−22.99	−22.24
z-coordinate of CoG, z_G [m]	−28.50	−31.96
Metacentric height, $\overline{GM}_0$ [m]	6.73	10.81
Displaced volume, V [m^3]	2.5986×10^3	2.9013×10^3
Buoy mass, m [kg]	2.6027×10^6	2.9140×10^6
Mom. inertia around x-axis at CoG, I_{xx} [kg m^2]	1.4437×10^9	1.5310×10^9
Mom. inertia around z-axis at CoG, I_{zz} [kg m^2]	0.1002×10^9	0.1118×10^9

Table 2: Validation parameters from Giorgi et al. [1]

Davidson et al., 2021 [3] provided a more detailed description of the device and its dimensions. A schematic representation of the geometry is presented in Figure 9. The dimensions of this geometry are presented in Table 2 for configuration D2.

The geometry created for the simulation is presented in Figure 10 The geometry presented in Figure 10 was created based on specific target parameters described in Davidson et al., 2021 [3]. The target parameters from the journal article and actual parameters of the final CAD geometry are presented in Table 3.

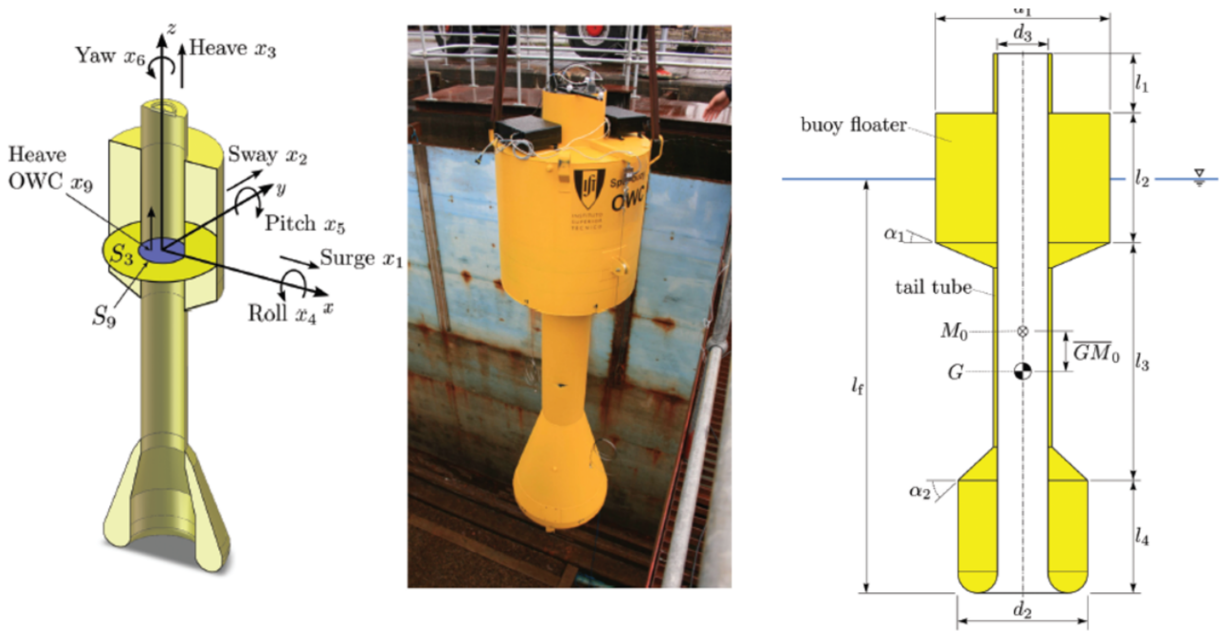

Figure 9: OWC device geometry. Taken from Davidson et al., 2021 [3]

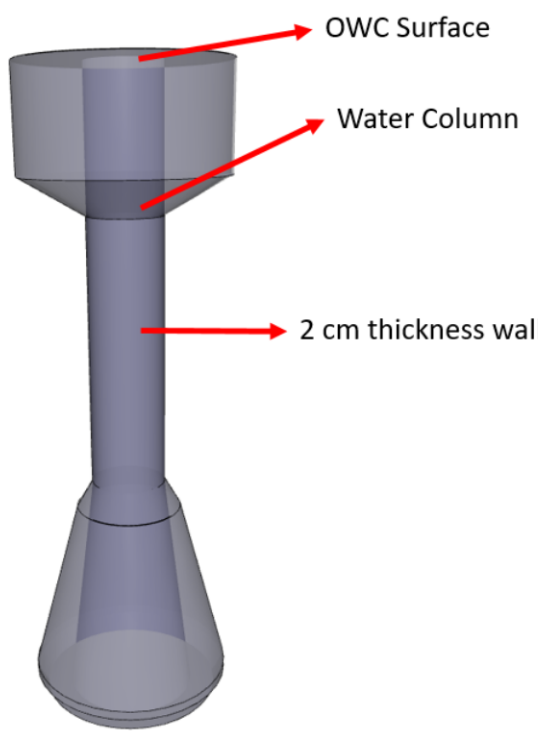

Figure 10: OWC CAD Geometry used for BEM simulations

Table 3: Target and actual properties for the OWC CAD geometry

Property	Target	Actual
Center of Buoyancy	-22.14 m	-22.05 m
Displaced Volume	2860 m^3	2858 m^3
Center of Mass	-31.96 m	-31.96 m

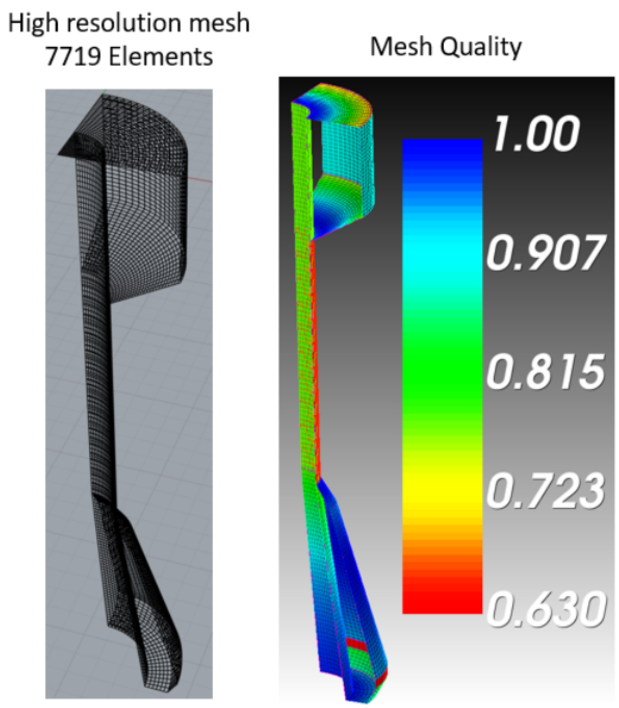

Figure 11: CUBIT Mesh and Mesh Quality for the GBM Simulation Approach

7.3.2 Mesh Development

The mesh was created using the software CUBIT 16.14, which is a software developed by Sandia Nationals Labs. The mesh created for this project and the mesh quality are presented in Figure 11. The mesh quality is defined as the aspect ratio of the mesh elements.

7.3.3 WAMIT Simulation

The BEM simulations for the GBM approach were developed in WAMIT, which allows to include additional degrees-of-freedom (DOFs) in the simulations. WAMIT has two options to include the additional DOFs: the first option is to use the separate script *defmod.f* that is included in the installation files for WAMIT. This option can be used just with the low order method. The other option is to use one of the subroutines available in the file *newmodes.f*, which can be used with both the low and high order methods. The first option was used for this project because it was easier to modify the *defmod.f* file. After modifying *defmod.f*, it is necessary to compile this file to create a .dll file, that will be used by WAMIT. The *defmod.f* contains the definition of the additional DOFs defined for the simulation. In this case, an additional DOF is added to the system, which is the vertical movement of the OWC. The BEMIO results for the GBM approach and the two-body approach are presented in Figures 12 and 13

Normalized Added Mass: $\bar{A}_{i,j}(\omega) = \dfrac{A_{i,j}(\omega)}{\rho}$

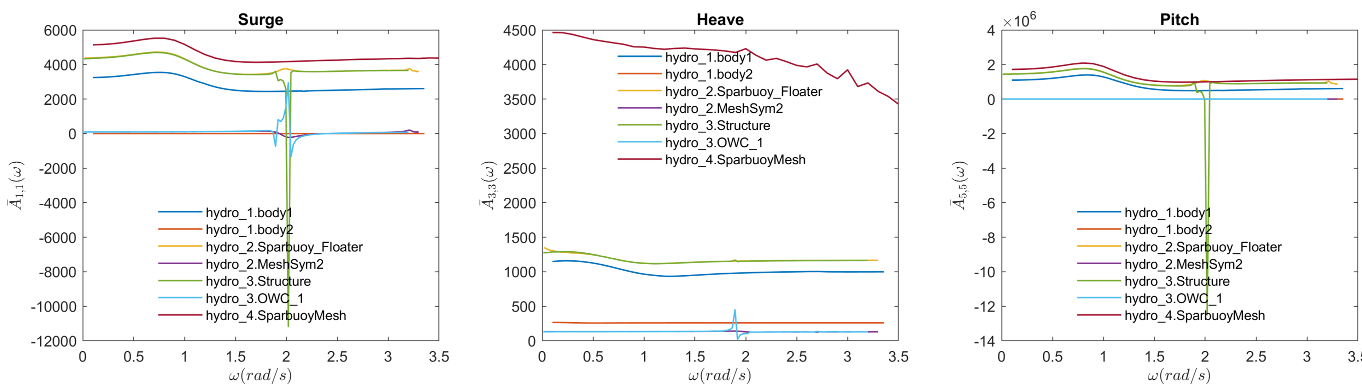

Notes:
- $\bar{A}_{i,j}(\omega)$ should tend towards a constant, A_∞, within the specified ω range.
- Only $\bar{A}_{i,j}(\omega)$ for the surge, heave, and pitch DOFs are plotted here. If another DOF is significant to the system, that $\bar{A}_{i,j}(\omega)$ should also be plotted and verified before proceeding.

(a) Added mass

Normalized Radiation Damping: $\bar{B}_{i,j}(\omega) = \dfrac{B_{i,j}(\omega)}{\rho\omega}$

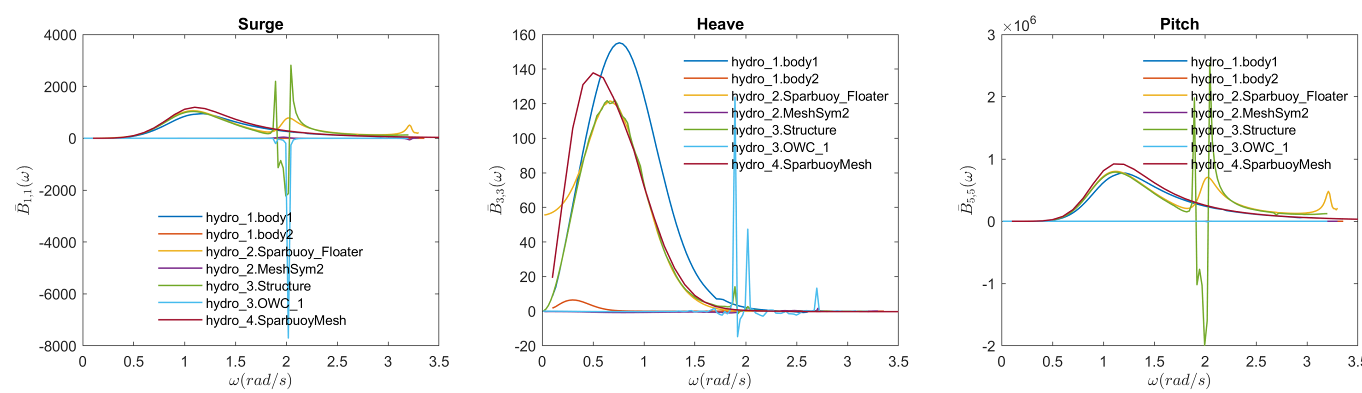

Notes:
- $\bar{B}_{i,j}(\omega)$ should tend towards zero within the specified ω range.
- Only $\bar{B}_{i,j}(\omega)$ for the surge, heave, and pitch DOFs are plotted here. If another DOF is significant to the system that $\bar{B}_{i,j}(\omega)$ should also be plotted and verified before proceeding.

(b) Radiation damping

Figure 12: WAMIT hydrodynamic coefficients compared for the GBM and two-body approach a) added mass and b) radiation damping

Normalized Radiation Impulse Response Functions: $\bar{K}_{i,j}(t) = \frac{2}{\pi}\int_0^\infty \frac{B_{i,j}(\omega)}{\rho}\cos(\omega t)d\omega$

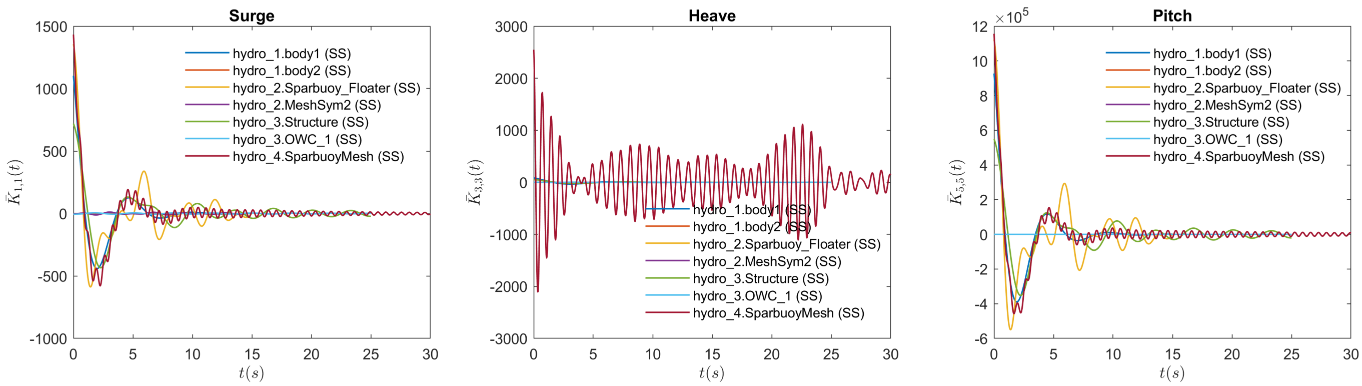

Notes:
- The IRF should tend towards zero within the specified timeframe. If it does not, attempt to correct this by adjusting the ω and t range and/or step size used in the IRF calculation.
- Only the IRFs for the surge, heave, and pitch DOFs are plotted here. If another DOF is significant to the system, that IRF should also be plotted and verified before proceeding.

(a) Radiation Impulse Reponse Function

Normalized Excitation Force Magnitude: $\bar{X}_i(\omega,\theta) = \frac{X_i(\omega,\theta)}{\rho g}$

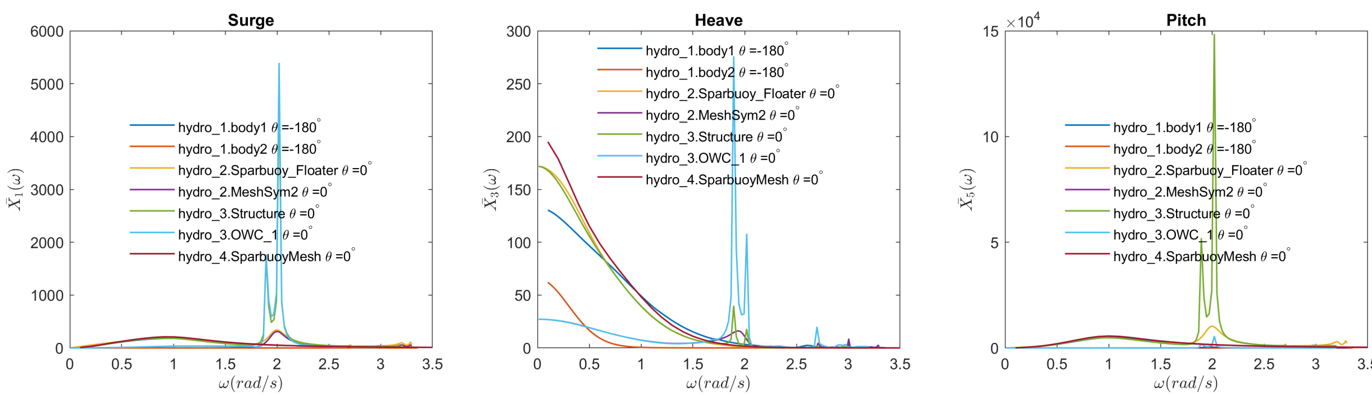

(b) Excitation Force Magnitude

Figure 13: WAMIT hydrodynamic coefficients compared for the GBM and two-body approach a) radiation impulse response function b) excitation force magnitude.

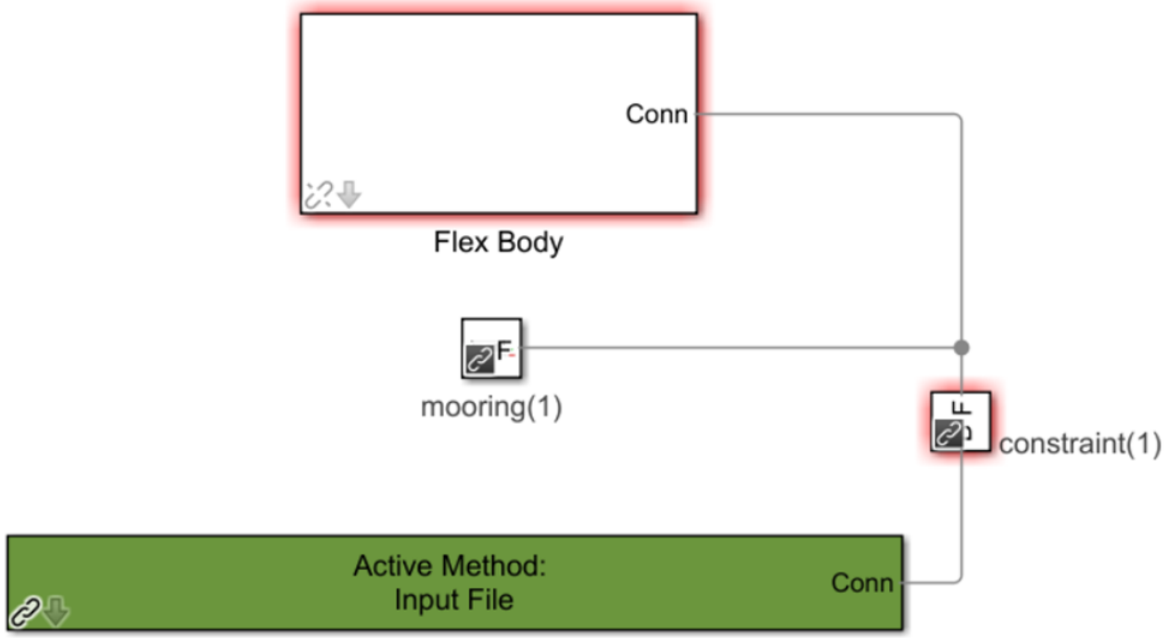

Figure 14: Top-level WEC-Sim model

7.3.4 WEC-Sim Implementation

After obtaining the BEM results for the GBM approach, a WEC-Sim model was developed. A top-level view of the implemented WEC-Sim model is presented in Figure 14. The Flexible Body block from WEC-Sim was used to model the OWC system using the GBM approach. In the GBM approach, an additional degree of freedom is added. In this case, the additional DOF for the system corresponds to the motion of the water column, which moves up and down inside the chamber, behaving like a piston. The GBM approach allows WEC-Sim to model this moving surface explicitly, capturing the piston's oscillatory motion and its interaction with the surrounding fluid dynamics. It is necessary to edit the default Flex Body block from the WEC-Sim library to account for the piston force. The force that is being modeled is presented in Equation 1.

$$F_{Piston} = v_{GBM} \frac{8\rho_{air} A_a^3}{\pi^2 C_d^2 d_0^2} |v_{GBM}| \tag{1}$$

In Equation 1, v_{GBM} is the velocity of the new DOF, ρ_{air} is the air density, A_a is the cross-sectional area of the air chamber, C_d is orifice discharge coefficient, and d_0 is the diameter of the orifice plate. The modified Flex Body block is shown in Figures 15 and 16.

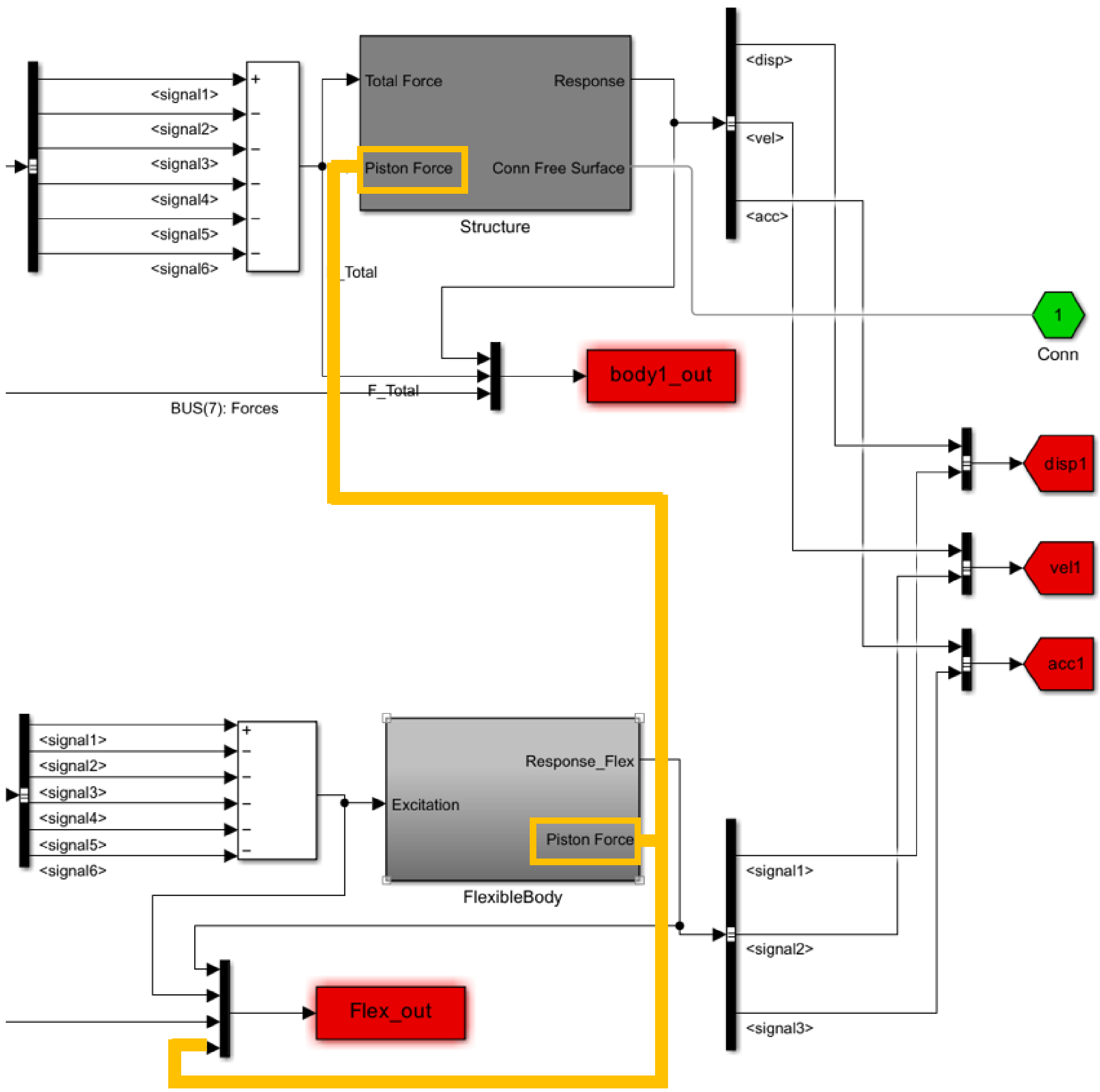

Figure 15: Modifications to the Flex Body block

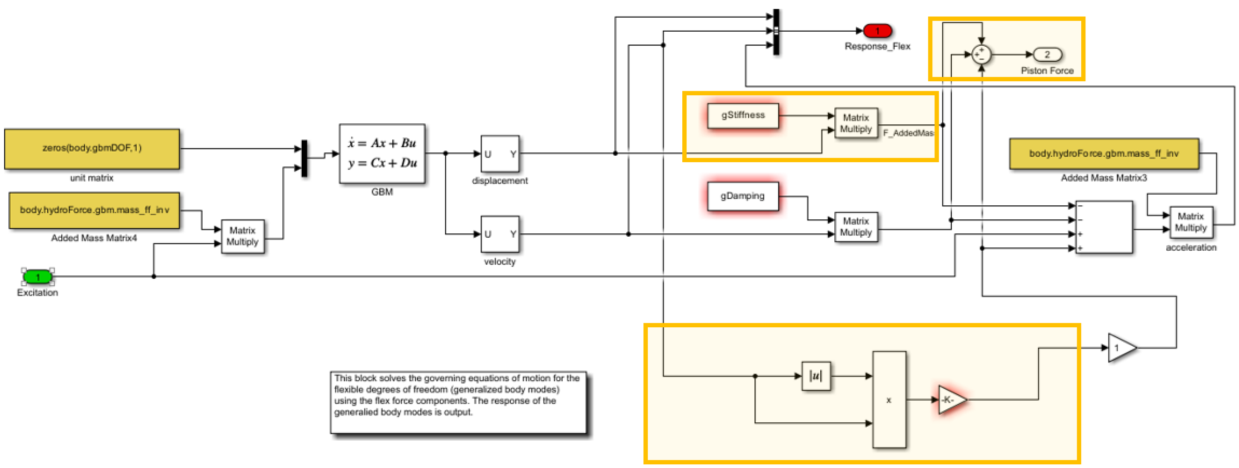

Figure 16: Piston force calculation in the Flex Body block

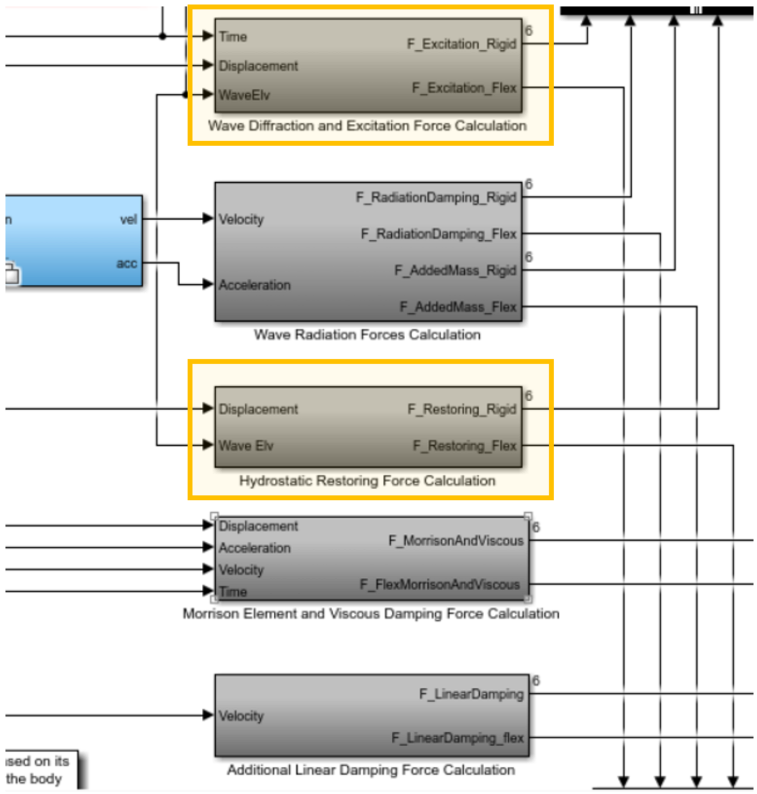

Figure 17: Subsystems in the Flex Body block from the WEC-Sim library that need to be modified

7.3.5 Non-linear hydrodynamics

The non-linear hydrodynamics of WEC-Sim are not currently available for the Flex Body block. In order to include the non-linear hydrodynamics option, it was necessary to edit two subsystems in the Flex Body block: *Wave Diffraction and Excitation Force Calculation* and the *Hydrostatic Restoring Force Calculation*, which are shown in Figure 17.

The subsystems highlighted in Figure 17 have the Nonlinear Froude-Krylov Force implementation and the nonlinear hydrostatic restoring force. The nonlinear functions receive as an input the displacement for the first 6 DOFs in the system. The Flex Body block has more than 6 DOFs, so it is necessary to edit the nonlinear subsystems use only the first 6 DOFs (and ignore the others). The modified nonlinear Froude-Krylov Force subsystem in the *Wave Diffraction and Excitation Force Calculation* block is presented in Figure 18. The modified nonlinear hydrostatic restoring Force subsystem in the *Hydrostatic Restoring Force Calculation* block is presented in Figure 19.

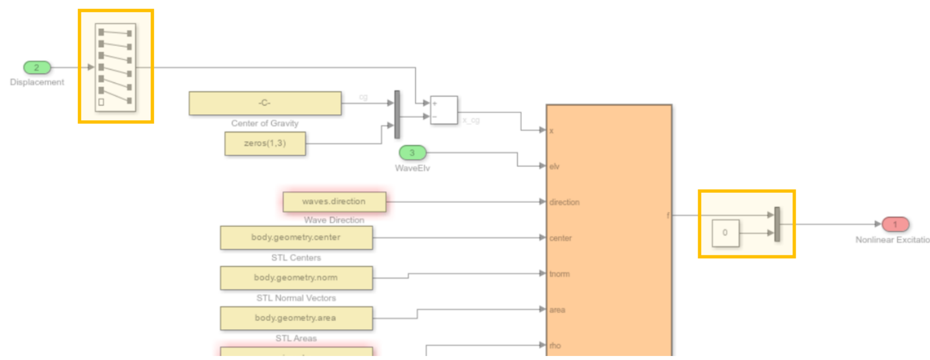

Figure 18: modified *Wave Diffraction and Excitation Force Calculation* block

7.4 WAVE-TO-WIRE CONTROL IMPLEMENTATION

Wave power is superior in its power density and consistency compared to other renewable energy resources, with the worldwide theoretical ocean energy potential estimated at 29.5 TWh/yr [4]. Wave energy generally has a higher energy flow per unit area, with an estimated energy density of 2–3 kW/m^2, higher than that of wind energy (0.4–0.6 kW/m^2) or solar energy (0.1–0.2 kW/m^2) [5]. However, designing wave energy converters (WECs) that are efficient and cost-effective presents significant challenges [6]. This complexity arises in part due to the variability and unpredictability of ocean wave dynamics, as well as the need to optimize power capture while ensuring structural durability in harsh marine environments. Moreover, integrating these devices into existing energy grids while maintaining cost-effectiveness and efficiency adds another layer of difficulty to the design process.

Control strategies are crucial for WECs, as they allow those devices to adapt to varying sea states and wave conditions in real time. By optimizing the response of WECs, those strategies can significantly enhance the amount of energy captured from waves. Recently, the wave energy research community highlighted the importance of developing controllers that integrate wave-to-wire (W2W) models [7, 8, 9] and control codesign methods [10, 11, 12] to maximize overall performance. Implementing control strategies with comprehensive knowledge of the dynamics of the PTO and electrical systems is challenging. In this context, OWCs are particularly appealing due to the well-understood dynamics of their gensets (the combination of a prime mover and an electrical generator used to produce electrical power), making OWCs one of the most promising WEC designs. To avoid losses associated with rectifying valves, the genset of an OWC contains a self-rectifying turbine, typically either a Wells or an axial radial/biradial flow impulse turbine. Zarketa et al. [13] demonstrated that the design of air turbines is also dependent on the characteristics of the OWC floater and controller. In this work, a Wells turbine is used.

Several optimal control approaches have been introduced in the literature and applied to fixed OWCs but have yet to be applied to a floating OWC. For example, in [14], a W2W approach was used to control a fixed OWC system with a bidirectional turbine. The study employed a model predictive control approach coupled with a Pontryagin's minimum principle optimizer to maximize electric energy generation. However, the authors demonstrated that the genetic-algorithm-optimized inverse fuzzy model control method described in [15] outperformed the tested model predictive control design for the specific OWC in the study.

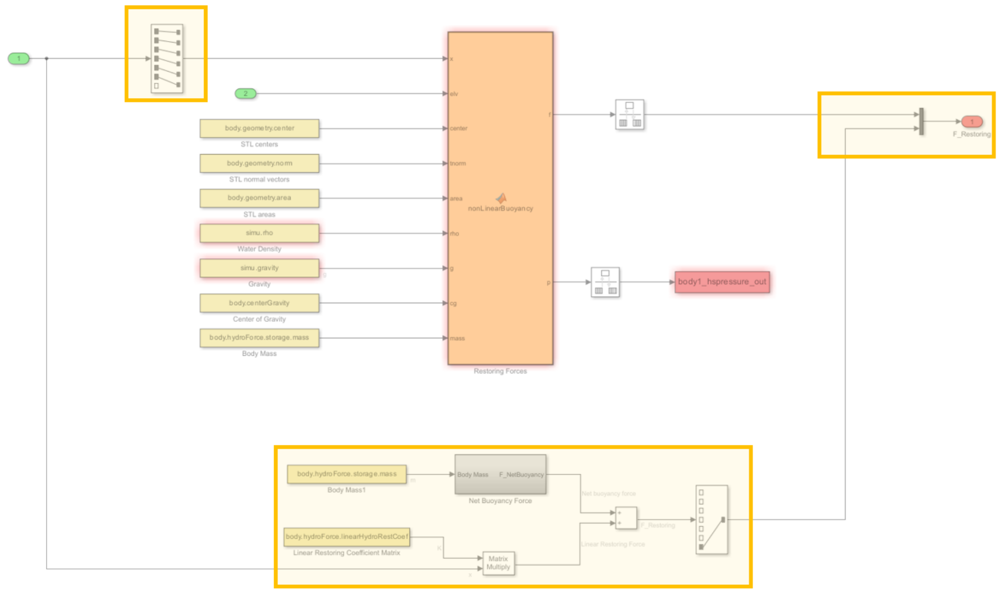

Figure 19: Modified *Hydrostatic Restoring Force Calculation* block

Rosati et al. [16] proposed a control strategy aimed at maximizing the overall W2W efficiency of fixed OWCs equipped with Wells turbines. Unlike traditional approaches that prioritize turbine efficiency, this strategy considers the entire OWC system. The control law was derived using a curve fitting technique to optimize power harvesting across various wave conditions, ensuring maximum average power output.

Unlike previous work in the literature, this study tests two optimal control methods on floating OWCs. The first method is the Turbine Efficiency Maximization (TEM) control described in [17], and the second is the W2W model developed in [16]. These two controllers were chosen due to their high performance, efficient computation, and the fact that they do not require excitation force estimation. In addition to this, the present report collects the main results presented in [18], which aims to test the potential benefits using both approaches to model floating OWC devices. The baseline for comparison will be the TEM approach, which has been used in previous studies with good results. The equations of motion of the air chamber, along with the performance curves of the generator set, were implemented in WEC-Sim, while MoorDyn was used to simulate the mooring forces.

7.4.1 Numerical Model

The floating OWC system in this study is modeled as a two-body system. The first body is the floater, while the second body represents the water column. The water column is constrained to heave-only motion relative to the floater's reference frame, as described in [1]. To simulate the response of both bodies to external forces, WEC-Sim v6.1 [19] was utilized. WEC-Sim is an open-source software specifically designed for simulating WECs. It is capable of modeling mooring dynamics, nonlinear hydrodynamics and drag forces, as demonstrated in [20] for a floating OWC. WEC-Sim can model both rigid and flexible bodies, making it particularly suited for the OWC system, which can be modeled either as a rigid body or using Generalized Body Modes (GBM) to account for free surface effects. This section describes the dynamic equation of the OWC system, mooring dynamics, air chamber dynamics and the performance curves of the turbine and generator.

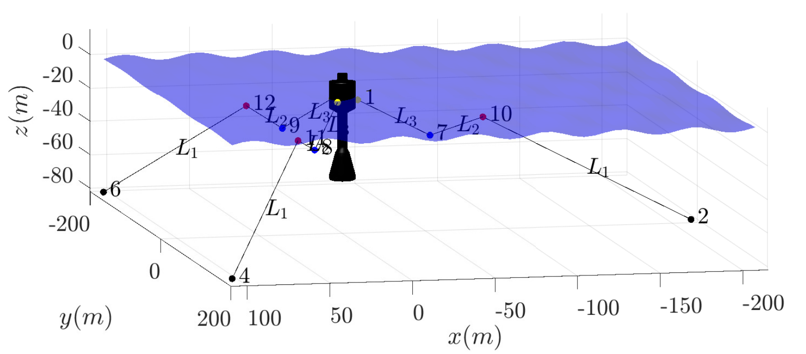

Figure 20: The floating OWC WEC and the mooring layout used in this study. The black dots represent anchoring points, the red dots are jumpers, and the blue dots represent the clump weights [18]

7.4.2 Floater and OWC dynamics

Both the rigid body approach and the GBM approach can be modeled using the following equation:

$$\boldsymbol{M}\ddot{\mathbf{x}} + \boldsymbol{D}\dot{\mathbf{x}} + \boldsymbol{K}_{\text{hs}}\mathbf{x} = \boldsymbol{Q}_{\text{ext}}^{\text{lin}} + \boldsymbol{Q}_{\text{ext}}^{\text{non}} + \boldsymbol{Q}_{\text{moor}} + \boldsymbol{Q}_{\text{rad}} + \boldsymbol{Q}_{\text{ch}} + \boldsymbol{Q}_{\text{drag}} \tag{2}$$

where $\mathbf{x} \in \mathbb{R}^n$ is a map for the system's heave displacement, and $\dot{\mathbf{x}}(t)$ and $\ddot{\mathbf{x}}(t) \in \mathbb{R}^{n\times 1}$ are the velocity and acceleration states, respectively. $\mathbb{R}$ is the set of real numbers, $n \in \mathbb{N}$ is the system's degrees of freedom, $\boldsymbol{M} \in \mathbb{R}^{n\times n}$ is the system's mass matrix, and $\boldsymbol{D}$ and $\boldsymbol{K}_{\text{hs}} \in \mathbb{R}^{n\times n}$ are the hydrodynamic radiation damping and hydrostatic stiffness matrices, respectively.

$\boldsymbol{Q}_{\text{ext}}^{\text{lin}}$ and $\boldsymbol{Q}_{\text{ext}}^{\text{non}} \in \mathbb{R}^{n\times 1}$ are the hydrodynamic linear and the nonlinear excitation forces, respectively, $\boldsymbol{Q}_{\text{moor}}\mathbb{R}^{n\times n}$ is the generalized mooring forces calculated using MoorDyn v2, $\boldsymbol{Q}_{\text{drag}}\mathbb{R}^{n\times 1}$ is the generalized viscous damping and hydrodynamic drag force, and $\boldsymbol{Q}_{\text{rad}} \in \mathbb{R}^{n\times 1}$ is the generalized radiation damping force as is expressed as [21]:

$$\boldsymbol{Q}_{\text{rad}} = -\boldsymbol{M}_{\infty}\ddot{\mathbf{x}} - \int_{-\infty}^{T} \boldsymbol{K}_{\text{r}}\, \dot{\mathbf{x}}\,(t-\tau)\, d\tau \tag{3}$$

where $\boldsymbol{M}_{\infty}$ is the generalized hydrodynamic added mass matrix and $\boldsymbol{K}_{\text{r}}$ is the radiation retardation function [22]. Finally, $\boldsymbol{Q}_{\text{ch}} \in \mathbb{R}^{n\times 1}$ is the generalized air chamber force and it is expressed as

$$\boldsymbol{Q}_{\text{ch}} = \left[A_{\text{ch}}\Delta p \mathbf{1}_3^T,\quad \mathbf{0}_{1\times 3},\quad -A_{\text{ch}}\Delta p\right]^T \tag{4}$$

where A_{ch} is the air chamber surface area, $\Delta p = p_{\text{ch}} - p_{\text{atm}}$ is the air chamber gauge pressure, p_{ch} and $p_{\text{atm}} \in \mathbb{R}$ are the air chamber absolute pressure and the atmospheric pressure at sea level, and $\mathbf{1}_3^T = [0\ 0\ 1]$. The dynamics of the air chamber are described in subsection 7.4.4.

7.4.3 Mooring system design

MoorDyn breaks each mooring line into equally sized segments connected by nodes. The mass of the line, as well as forces like gravity, buoyancy, hydrodynamic loads and seabed reactions are concentrated at these nodes. Hydrodynamic effects such as drag and added mass are computed using Morison's equation. The axial stiffness of the line is modeled by applying tension to each segment, with a linear stiffness response, while a damping term is added to reduce artificial resonances caused by the lumped-mass approach. Bending and torsional stiffnesses are not included. When a node falls below the seabed, vertical stiffness and damping forces are applied to simulate seabed contact.

Figure 20 shows the mooring system layout defined in MoorDyn v2. The float is connected to the mooring lines at the yellow dots, located at $z_F = 2.58$ m, measured from the free surface. The jumper (riser) and clump weights' mass and density were tuned to achieve the desired stiffness for the mooring system. Table 4 summarizes the properties of the mooring system [1].

7.4.4 Air Chamber dynamics

The air chamber is bounded by the water free surface from below, the turbine and the float internal walls from above and on the sides. The rate of change of the air chamber pressure is computed as in [16]:

$$\Delta\dot{p} = -\left(\Delta p + p_{\text{atm}}\right)\frac{\gamma}{V_{\text{ch}}}\left(\dot{V}_{\text{ch}} + \frac{\Delta p\, d_{\text{turb}}}{k\,\Omega\,\rho_{\text{ch}}}\right) \tag{5}$$

where $\gamma = 1.4$ is the specific heat ratio, $V_{\text{ch}}(t) = V_0 - A_{\text{ch}}x_7(t) \in \mathbb{R}$ is the air chamber instantaneous volume, $V_0 = A_{\text{ch}}h_{\text{ch}} \in \mathbb{R}$ is the initial air chamber volume, h_{ch} is the initial chamber height, $x_7 \in \mathbb{R}$ is the OWC heave motion relative to the float reference frame, $d_{\text{turb}} \in \mathbb{R}_+$ is the turbine diameter, $\Omega \in \mathbb{R}_+$ is the turbine rotational speed, $k \in \mathbb{R}_+$ is the turbine geometric coefficient (explained in subsection 7.4.6), and ρ_{ch} is the instantaneous air chamber density, computed as:

$$\rho_{\text{ch}} = \rho_{\text{atm}}\left(p_{\text{ch}}/p_{\text{atm}}\right)^{\frac{1}{\gamma}} \tag{6}$$

7.4.5 Genset Model

The genset comprises the turbine and generator, which are directly coupled without a gearbox. This configuration ensures that the rotational speed of the turbine matches that of the generator, facilitating efficient energy conversion and reduces the maintenance required for the gearbox.

Table 4: Mooring system parameters [18].

Parameter	Value
Line properties	
Line diameter, d_L (mm)	32
Line density, w_L (kg/m)	34.82
Line stiffness, k_L (N)	1.5×10^6
Line internal damping, c_L (Ns)	-0.8
Line bent stiffness, $k_{bent,L}$ (Nm^2)	1×10^4
Transverse drag coefficient, C_d	1.6
Transverse added mass coefficient, C_a	1.0
Tangential drag coefficient, $C_{d,Ax}$	0.5
Tangential added mass coefficient, $C_{a,Ax}$	0.5
Attachment properties	
Jumper mass, m_J (kg)	4030.46
Jumper density, ρ_J (kg/m^3)	123.00
Clump-weight mass, m_C (kg)	36139.83
Clump-weight density, ρ_C (kg/m^3)	8097.50
Anchor radius, r_A (m)	211.2
Anchor z-coordinate, z_A (m)	-80
Fairlead z-coordinate, z_F (m)	-2.58
Fairlead radial coordinate, r_F (m)	9.28
Segment lengths	
Length of line anchor-jumper, L_1 (m)	143.28
Length of line jumper-clump-weight, L_2 (m)	37.01
Length of line fairlead-clump-weight, L_3 (m)	50.40

7.4.6 Turbine Performance

The turbine performance can be described by the following dimensionless coefficients:

$$\Phi = \frac{w_{\text{turb}}}{\rho_{\text{in}}\Omega d_r^3}, \Pi = \frac{P_{\text{turb}}}{\rho_{\text{in}}\Omega^3 d_r^5}, \Psi = \frac{\Delta p}{\rho_{\text{in}}\Omega^2 d_r^2} \times s \tag{7}$$

where $\Psi \in \mathbb{R}$ is the turbine dimensionless head which acts as the input for the performance curves described in Figure 21, and $\Phi \in \mathbb{R}$ and $\Pi \in \mathbb{R}_+$ are the dimensionless mass flow rate and turbine power. Note that Φ is

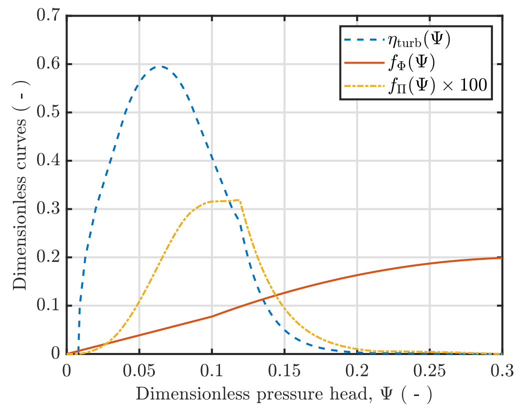

Figure 21: Turbine performance curves [16]

an odd function and Π is an even function, and $\rho_{in} = \max(\rho_{ch}, \rho_{atm})$. s is a safety parameter, in which $s = 0$ indicates that $\Omega > \Omega^{max}$, otherwise $s = 1$.

The rotational speed of the turbine (and the generator) is described as follows,

$$\frac{d}{dt}\left(\frac{1}{2}I_{turb}\Omega^2\right) = P_{turb} - u\,\Omega - L_{friction} \tag{8}$$

where $I_{turb} \in \mathbb{R}_+$ is the turbine moment of inertia, $P_{turb} \in \mathbb{R}_+$ is the turbine power, u is the control torque, and $L_{friction}$ represents the friction losses in the genset. In this work, $L_{friction}$ is neglected and Eq. (8) can be expressed as:

$$\dot{\Omega} = (T_{turb} - u)\,/I_{turb} \tag{9}$$

where $T_{turb} \in \mathbb{R}_+$ is the turbine torque.

The turbine geometric parameter k is a function of the hub-to-tip diameter ratio and the total bladed area divided by annular area (solidity ratio), and it is expressed as $k = \Psi/\Phi$.

7.4.7 Generator Performance and Power

The rotational speed of the turbine is same as the generator. Silva et al. [23] described the generator power as a function of the rotational speed and control torque:

$$\begin{aligned}P_{gen}(\Omega, T_{turb}) = {} & 6.280 \times 10^{-10}\Omega^5 - 1.003 \times 10^{-6}\Omega^4 \\ & + 4.416 \times 10^{-4}\Omega^3 - 0.07028\,\Omega^2 + 2.106\,\Omega \\ & - 0.06941\,T_{ctrl}^2 - 6.014\,T_{ctrl} - 4.664 \times 10^{-8}\Omega^4 T_{ctrl} \\ & + 1.79 \times 10^{-8}\Omega^3 T_{ctrl}^2 + 2.089 \times 10^{-5}\Omega^3 T_{ctrl} \\ & - 9.816 \times 10^{-6}\Omega^2 T_{ctrl}^2 - 0.003354\,\Omega^2 T_{ctrl} \\ & + 0.001292\,\Omega T_{ctrl}^2 + 1.189\Omega T_{ctrl} - 139.3\end{aligned} \tag{10}$$

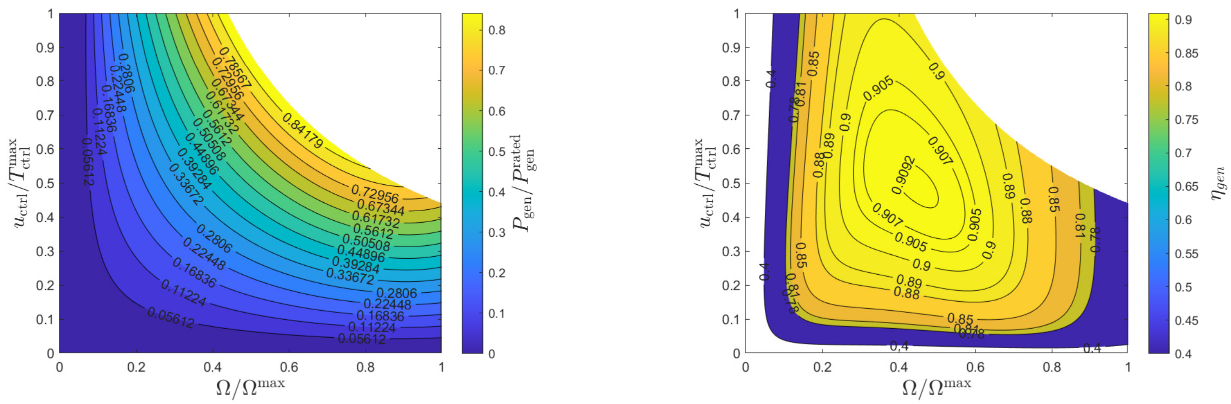

(a) Generator Dimensionless Power

(b) Generator Efficiency

Figure 22: Generator Efficiency and Power Performance Curves [23]

Eq. (10) can be used to generate Figure 22, in which the generator rated power $P^{\mathrm{rated}}_{\mathrm{gen}} = 30$ KW and the efficiency is expressed as $\eta = P_{\mathrm{gen}}/P_{\mathrm{turb}}$.

7.4.8 Optimal Control

Numerous optimal control methods for OWCs have been proposed in the literature. This work is focused on two existing approaches to tackle the optimal control problem. The first method ensures that the turbine operates at maximum efficiency, while the second method employs a W2W control strategy to maximise the W2W generation. Both algorithms pose a low computational burden.

To optimize the performance, the rotational speed of the turbine must align with the available pneumatic energy, specifically the standard deviation of the pressure oscillations (σ_Ψ). As demonstrated in [24, 13], turbine efficiency is influenced by this standard deviation, with maximum efficiency occurring at specific values for different turbine types. For example, the optimal standard deviation for the Wells turbine is $\sigma_{\Psi_{\max}} = 0.022$. The relationship between torque and turbine speed follows a quadratic form given by:

$$u_{\mathrm{TEM}} = a_0 \Omega^{a_1 - 1} \tag{11}$$

where $a_0 = \rho_{\mathrm{air}} d_r^5 \Pi \approx 2 \times 10^{-4}$ and $a_1 = 3$. The second control approach used in this paper was introduced in [16] for a Wells turbine in a fixed OWC, consisting of two components: a global setpoint derived from the entire W2W model and a Lyapunov-based nonlinear controller to track this setpoint. The control torque for this model is expressed as:

$$u_{\mathrm{W2W}} = \frac{b_0 + b_1 \Omega + b_2 \exp^{b_3 \Omega}}{\Omega} \tag{12}$$

where $b_0 = 136$, $b_1 = 0.739$, $b_2 = 1.2$, and $b_3 = 0.034$. When the genset speed is low, the linear part dominates the control signal, and, at high speeds, the exponential part dominates the control signal.

Parameter	Value	Units
d_r	0.75	m
I_{hub}	3.06	kg m^2
$\Omega^{\max}$	350	rad/sec
$u^{\max}$	216.5	N.m
γ	1.4	J/(kg K)
h_{ch}	4.5	m
d_{ch}	5.89	m

Table 5: Turbine and air chamber parameters [18].

The coefficients b_i in Eq. (12) are determined using a straightforward curve fitting approach [18]. In this method, the genset speed is plotted against the average electrical power generated under various wave conditions. The maximum average power points are then identified for each wave condition and a curve that satisfies Eq. (12) is chosen. While this control approach is fast to implement and poses low computational burden, it requires multiple *a priori* offline simulations to generate the curves necessary for the curve fitting process.

7.4.9 Results and Discussion

This report investigates the performance of two optimal control approaches on a floating spar-buoy OWC. Ansys Aqwa was used to simulate the floating OWC using the two rigid-body approach. The built-in WEC-Sim libraries were employed to simulate the OWC as two rigid bodies, and the air chamber, turbine and generator models were modeled in Simulink. The control approaches were tested in irregular waves using the Pierson-Moskowitz Spectrum with a significant wave height of 4.5 m, a peak period of 11.2 seconds and a ramping time of 60 seconds. The turbine's initial rotational speed was set to 150 rad/sec. Table 5 lists the values used for the turbine parameters and the air chamber.

Figure 23 shows the heaving states for the floater and the OWC, the air chamber pressure, and the turbine speed, from top to bottom. It can be seen that the heaving response for both controllers is almost identical. However, the air chamber pressure differs slightly during large wave peaks. During periods of low excitation, the TEM controller maintains lower turbine speed to keep it in an efficient zone of operation. On the other hand, the W2W controller maximizes the useful electrical power which can be increased with larger turbine velocity (despite lower turbine efficiency) and vise versa.

Figure 24 shows the pneumatic power available in the system as a result of each controller, along with the turbine and generator power. It can be observed that both control methods behave similarly when there is little pneumatic power available in the system. However, when a large pneumatic power is present, the W2W approach harvests more energy, with average generator efficiency of 70.36% compared to 61.74% for the TEM control.

When integrating the generator power curves with respect to time, the generated energy is obtained, as illustrated in Figure 25. The W2W control harvested 30.2% more energy compared to the TEM control.

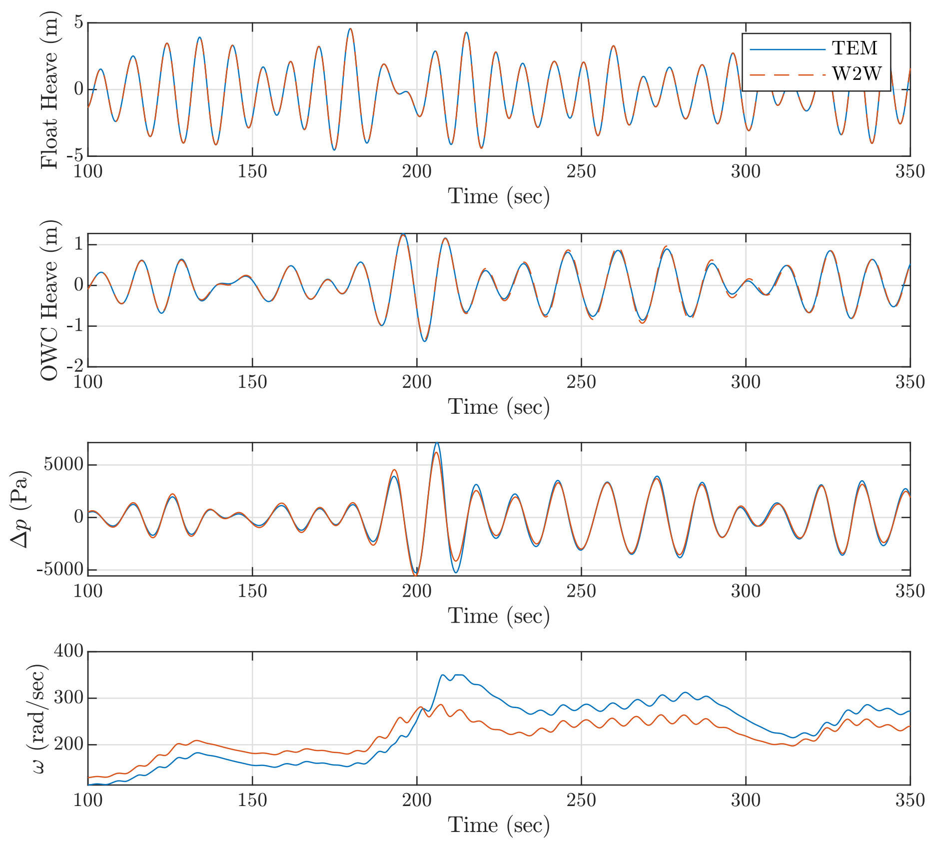

Figure 23: Floating OWC system heave, pressure, and turbine velocity states [18].

The W2W control favours the system overall efficiency and power over the turbine efficiency.

7.4.10 Conclusions

This study investigates two of the control methods presented in the literature for a floating OWC, taking into account the hydrodynamic interaction between the float and the water column, the dynamics of the mooring lines, and the effects of quadratic viscous forces. Additionally, the air chamber, turbine, and generator models were implemented in the open-source software WEC-Sim.

Among the two control approaches, one aimed at maximizing turbine efficiency, while the second focused on maximizing the overall W2W energy conversion. The two control approaches were chosen as they do not require excitation force estimation. It was observed that, under the tested wave conditions, the harvested energy was 30% greater for the W2W control approach. The results highlight the importance of

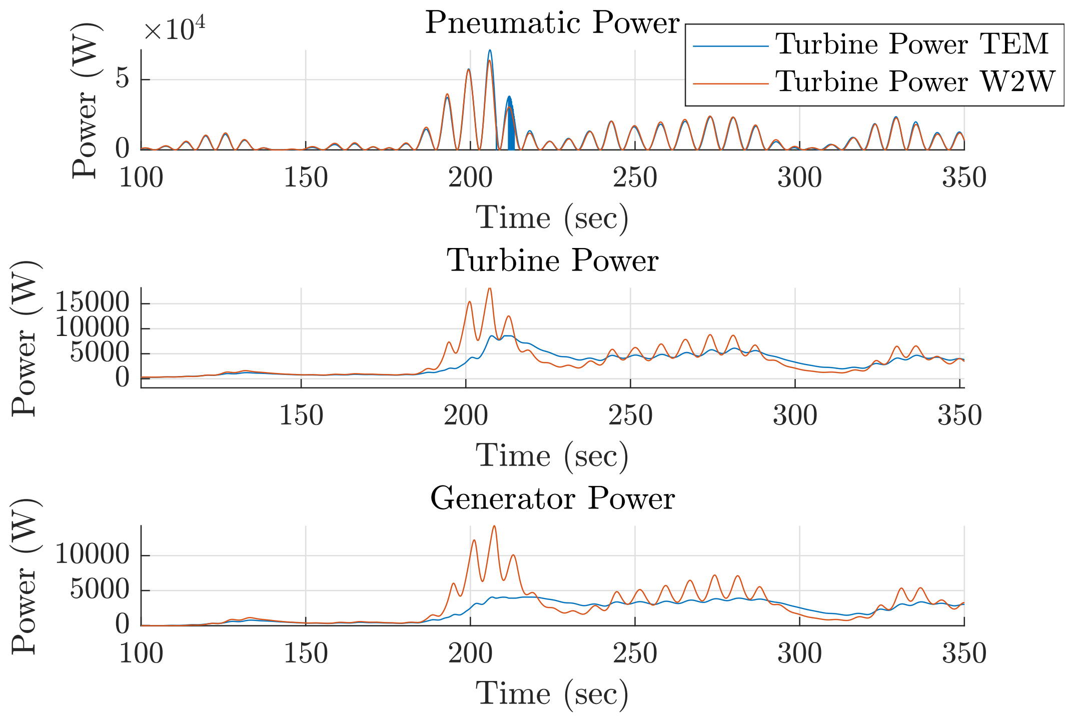

Figure 24: Pneumatic, turbine, and generator power [18].

implementing W2W control for floating OWCs and underscore the significance of codesign in developing such devices.

8 LESSONS LEARNED AND TEST PLAN DEVIATION

8.1 LESSONS LEARNED

Throughout the project, several insights emerged that can guide future efforts in developing advanced numerical models for OWC systems:

- **Importance of Mesh Quality**: One of the primary lessons learned was the impact of mesh quality on model stability and accuracy, especially for nonlinear hydrodynamics in WEC-Sim. Initial attempts with a coarser mesh led to significant model instability, demonstrating that fine-tuning mesh parameters is essential for reliable simulation outputs. Future projects should allocate sufficient time to optimize mesh resolution, balancing computational speed and accuracy.

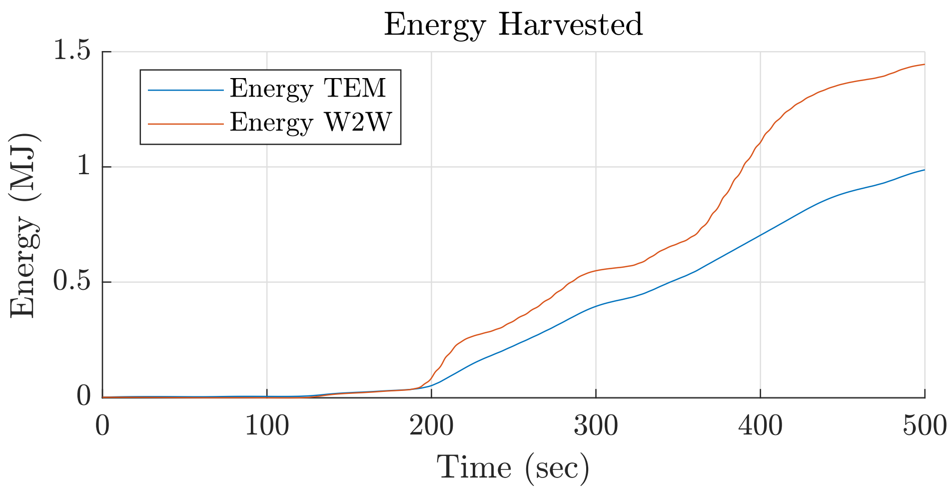

Figure 25: Harvested Electric Energy [18].

- **Nonlinear Hydrodynamic Limitations**: Implementing nonlinear hydrodynamics presented challenges, as this functionality led to non-physical drift in certain degrees of freedom, even with refined meshes. This outcome emphasized the limitations within current modeling approaches for capturing complex nonlinearities. Further development or integration of specialized hydrodynamic modules could enhance future model performance.
- **Performance of Control Algorithms**: Testing both Turbine Efficiency Maximization (TEM) and Wave-to-Wire (W2W) control strategies showed that W2W control is significantly better at capturing energy. However, W2W requires more precise adjustments to align turbine speed with changing wave conditions. This finding highlights the potential of W2W control for improving energy capture. However, it also suggests that simpler methods for fine-tuning could help make W2W more practical to use.
- **Collaborative Data Management and Documentation**: Keeping data organized and well-documented was key to keeping everyone on the same page, especially when multiple teams were involved. Storing WEC-Sim data in easy-to-access formats and using a clear version-tracking system helped the project run smoothly and will be valuable practices for future team projects.

8.2 TEST PLAN DEVIATION

While the project adhered closely to the original test plan, a few deviations were necessary to address unforeseen challenges and optimize model performance:

- **Extended Testing of Nonlinear Hydrodynamics**: Stability issues in nonlinear hydrodynamics due to mesh quality and non-physical drift required additional testing iterations and adjustments. As a result, the team deferred some nonlinear testing and conducted comparative studies with linear models to proceed with reliable data.

- **Simplification of Initial Control Tests**: Due to complexity in tuning the W2W control, early control tests used a simplified version of the TEM control strategy as a baseline for validation. This step allowed the team to establish a stable control framework before integrating the more complex W2W algorithm, leading to more consistent outcomes and a successful comparison of control strategies.
- **Deferred Nonlinearities in GBM Approach**: When testing the Generalized Body Mode (GBM) approach, it became evident that including nonlinear hydrodynamics in this configuration required more extensive modifications to the WEC-Sim source software than anticipated. Therefore, the team focused on linear results for the GBM model, with plans to revisit nonlinear effects in future model versions.

These changes gave us useful insights, helping to build a strong, well-documented model and showing areas to improve in future projects. The lessons learned and updates to the test plan made the results stronger, creating a solid base for Mondragon University's continued research in wave energy systems.

8.3 FUTURE WORK

Acknowledgment

This research was supported by the U.S. Department of Energy's Water Power Technologies Office. The authors would like to acknowledge funding support from the Testing & Expertise for Marine Energy (TEAMER) program: https://teamer-us.org/. Sandia National Laboratories is a multi-mission laboratory managed and operated by National Technology and Engineering Solutions of Sandia, LLC., a wholly owned subsidiary of Honeywell International, Inc., for the U.S. Department of Energy's National Nuclear Security Administration under contract DE-NA0003525. This report describes objective technical results and analysis. Any subjective views or opinions that might be expressed in the report do not necessarily represent the views of the U.S. Department of Energy or the United States Government.

References

[1] G. Giorgi, R. P. Gomes, J. C. Henriques, L. M. Gato, G. Bracco, and G. Mattiazzo, "Detecting parametric resonance in a floating oscillating water column device for wave energy conversion: Numerical simulations and validation with physical model tests," *Applied Energy*, vol. 276, p. 115421, 2020. [Online]. Available: https://www.sciencedirect.com/science/article/pii/S0306261920309338

[2] R. Gomes, J. Henriques, L. Gato, and A. Falcão, "Hydrodynamic optimization of an axisymmetric floating oscillating water column for wave energy conversion," *Renewable Energy*,

vol. 44, pp. 328–339, 2012. [Online]. Available: https://www.sciencedirect.com/science/article/pii/S0960148112001413

[3] J. Davidson, J. C. C. Henriques, R. P. F. Gomes, and R. Galeazzi, "Opening the air-chamber of an oscillating water column spar buoy wave energy converter to avoid parametric resonance," *IET Renewable Power Generation*, vol. 15, no. 14, pp. 3109–3125, 2021. [Online]. Available: https://ietresearch.onlinelibrary.wiley.com/doi/abs/10.1049/rpg2.12204

[4] O. Edenhofer, *Renewable energy sources and climate change mitigation: Special report of the intergovernmental panel on climate change*. Cambridge University Press, 2011.

[5] H. Wang, J. Sun, Z. Xi, S. Dai, F. Xing, and M. Xu, "Recent progress on built-in wave energy converters: A review," *Journal of Marine Science and Engineering*, vol. 12, no. 7, 2024. [Online]. Available: https://www.mdpi.com/2077-1312/12/7/1176

[6] B. Guo and J. V. Ringwood, "A review of wave energy technology from a research and commercial perspective," *IET Renewable Power Generation*, vol. 15, no. 14, pp. 3065–3090, 2021.

[7] X. Zhou, S. Zou, W. W. Weaver, and O. Abdelkhalik, "Assessment of electrical power generation of wave energy converters with wave-to-wire modeling," *IEEE Transactions on Sustainable Energy*, vol. 13, no. 3, pp. 1654–1665, 2022.

[8] M. Penalba and J. V. Ringwood, "A high-fidelity wave-to-wire model for wave energy converters," *Renewable energy*, vol. 134, pp. 367–378, 2019.

[9] J. Tan, W. Tao, A. J. Laguna, H. Polinder, Y. Xing, and S. Miedema, "A spectral-domain wave-to-wire model of wave energy converters," *Applied Ocean Research*, vol. 138, p. 103650, 2023. [Online]. Available: https://www.sciencedirect.com/science/article/pii/S0141118723001918

[10] H. Abdulkadir and O. Abdelkhalik, "Control co-design optimization of nonlinear wave energy converters," *Ocean Engineering*, vol. 304, p. 117827, 2024. [Online]. Available: https://www.sciencedirect.com/science/article/pii/S002980182401165X

[11] C. A. M. Ströfer, D. T. Gaebele, R. G. Coe, and G. Bacelli, "Control co-design of power take-off systems for wave energy converters using wecopttool," *IEEE Transactions on Sustainable Energy*, vol. 14, no. 4, pp. 2157–2167, 2023.

[12] J. A. Leon-Quiroga, G. Bacelli, D. D. Forbush, S. J. Spencer, and R. G. Coe, "An efficient and effective wec power take-off system," *IEEE Transactions on Sustainable Energy*, vol. 14, no. 3, pp. 1526–1539, 2023.

[13] A. Zarketa-Astigarraga, A. Martin-Mayor, A. Measo, B. D. Miguel, M. Martinez-Agirre, and M. Penalba, "A holistic optimization tool for the design of power take-off systems in realistic wave climates : The wells turbine case," *Ocean Engineering*, vol. 285, p. 115332, 2023. [Online]. Available: https://doi.org/10.1016/j.oceaneng.2023.115332

[14] J. Marques Silva, S. M. Vieira, D. Valério, and J. C. Henriques, "Model predictive control based on air pressure forecasting of owc wave power plants," *Energy*, vol. 284, p. 129217, 2023. [Online]. Available: https://www.sciencedirect.com/science/article/pii/S0360544223026117

[15] J. M. Silva, S. M. Vieira, D. Valério, and J. C. Henriques, "Ga-optimized inverse fuzzy model control of owc wave power plants," *Renewable Energy*, vol. 204, pp. 556–568, 2023. [Online]. Available: https://www.sciencedirect.com/science/article/pii/S0960148123000514

[16] M. Rosati, H. A. Said, and J. V. Ringwood, "Wave-to-wire control of an oscillating water column wave energy system equipped with a wells turbine," in *Proceedings of the 15th European wave and tidal energy conference*, 2023.

[17] J. Henriques, J. Portillo, W. Sheng, L. Gato, and A. d. O. Falcão, "Dynamics and control of air turbines in oscillating-water-column wave energy converters: Analyses and case study," *Renewable and Sustainable Energy Reviews*, vol. 112, pp. 571–589, 2019.

[18] M. A. Shabara, J. Leon-Quiroga, J. Grasberger, Y. Peña-Sanchez, and M. Penalba, "Optimal control of floating oscillating water column wave energy converters," in *The 9th IEEE Conference on Control Technology and Applications (CCTA)*, 2025.

[19] "Wec-sim v6.1," September 2024. [Online]. Available: https://doi.org/10.5281/zenodo.13770349

[20] M. Penalba, A. Zarketa, G. Giorgi, and Y. Peña-Sánchez, "Nonlinear hydrodynamic modelling for floating wave energy converters: A code-to-code comparison," in *Trends in Renewable Energies Offshore*, C. G. Soares, Ed. Taylor & Francis, 2022, pp. 319–328.

[21] M. A. Shabara and O. Abdelkhalik, "Optimal control of variable-shape wave energy converters," *IEEE Control Systems Letters*, vol. 7, pp. 1333–1338, 2023.

[22] Mohamed A. Shabara and Ossama Abdelkhalik, "Dynamic modeling of the motions of variable-shape wave energy converters," *Renewable and Sustainable Energy Reviews*, vol. 173, p. 113070, 2023. [Online]. Available: https://www.sciencedirect.com/science/article/pii/S1364032122009510

[23] J. M. Silva, S. M. Vieira, D. Valério, and J. C. Henriques, "Model predictive control based on air pressure forecasting of owc wave power plants," *Energy*, vol. 284, p. 129217, 2023. [Online]. Available: https://doi.org/10.1016/j.rser.2022.113070

[24] A. F. Falcão and J. C. Henriques, "Oscillating-water-column wave energy converters and air turbines: A review," *Renewable Energy*, vol. 85, pp. 1391–1424, 2016. [Online]. Available: https://www.sciencedirect.com/science/article/pii/S0960148115301828